Paracrine FGF21 dynamically modulates mTOR signaling to regulate thymus function across the lifespan

Sarah A. Wedemeyer[1], Nicholas E. Jones[1], Iwan G. A. Raza[2], Freedom M. Green[1], Yangming Xiao[1], Manpreet K. Semwal[3,4], Aaron K. Garza[1], Kahealani S. Archuleta[1], Kymberly L. Wimberly[1], Thomas Venables[5], Georg A. Holländer[6-8], Ann V. Griffith[1,3*]

[1]Department of Microbiology, Immunology, & Molecular Genetics, UT Health San Antonio, San Antonio, TX, USA

[2]Medical Sciences Division, University of Oxford, Oxford, UK

[3]Sam and Ann Barshop Institute for Aging and Longevity Studies, UT Health San Antonio, San Antonio, TX, USA

[4]Current address: Department of Math and Science, Our Lady of the Lake University, San Antonio, TX, USA

[5]Herbert Wertheim UF Scripps Institute for Biomedical Innovation & Technology, Jupiter, FL, USA

[6]Institute of Developmental and Regenerative Medicine, Department of Paediatrics, University of Oxford, Oxford, UK

[7]Paediatric Immunology, Department of Biomedicine, University of Basel and University Children's Hospital, Basel, Switzerland

[8]Developmental Immunology, Department of Biosystems and Engineering, ETH Zurich, Switzerland

***Correspondence:** Ann V. Griffith griffitha3@uthscsa.edu

Keywords: FGF21, thymus, thymic stromal cells, mTEC, cTEC, mTOR, paracrine signaling, thymus atrophy

Running Title: Paracrine FGF21 prolongs thymus function

Summary

Consequences of age-associated thymic atrophy include declining T cell responsiveness to pathogens and vaccines, and diminished T cell self-tolerance. Cortical thymic epithelial cells (cTECs) are primary targets of thymic aging, and recent studies suggested that their maintenance requires mTOR signaling downstream of medullary TEC (mTEC)-derived growth factors. To test this hypothesis, we generated a knock-in (KI) mouse model in which FGF21 and mCherry are expressed by most mTECs. We find that mTEC-derived FGF21 promotes temporally distinct patterns of mTORC1 and mTORC2 signaling in cTECs, promotes thymus and individual cTEC growth and maintenance, increases T cell responsiveness to viral infection, and diminishes indicators of peripheral autoimmunity in older mice. The effects of FGF21 overexpression on thymus size and mTOR signaling were abrogated by treatment with the mTOR inhibitor rapamycin. These results reveal a mechanism by which paracrine FGF21 signaling regulates thymus size and function throughout the lifespan, as well as potential therapeutic targets for improving T cell function and tolerance in aging.

Introduction

T lymphocytes are critical mediators of the adaptive immune response that require continuous replenishment. New T cells are generated in the thymus by periodic recruitment of thymus seeding progenitors[1, 2]. Mutually inductive signaling in the unique stromal microenvironment of the thymus directs these multi-potent progenitors along a program of differentiation, proliferation, and selection to generate a self-tolerant, self-restricted T cell population[3, 4, 5]. The stromal microenvironment is comprised of various types of thymic epithelial cells (TECs) as well as mesenchymal, neural, vascular, and non-lymphoid hematopoietic populations. TECs generate most of the known inductive signals required for T cell differentiation in the thymus, as well as a variety of factors which regulate the spatial migration of progenitors through the thymus[3, 6].

Rearrangement of T cell receptor (TCR) gene segments during T cell development allows the generation of a panoramic spectrum of TCR specificities to facilitate the recognition of diverse antigens[7]. This diversity depends on the number of T cells generated in the thymus. However, thymic output in humans is estimated to peak during the first few years of life, but decline by around 75% by middle age[8, 9, 10, 11, 12, 13], resulting in impaired production of new, naïve T cells[14, 15] and a diminished TCR diversity driven by the compensatory proliferation of memory T cells[16, 17, 18, 19]. Resulting immunodeficiencies include decreased vaccine responsiveness and tumor surveillance[20], as well as diminished response to infection[21, 22] (reviewed in[23]). Not only does a smaller pool of naïve T cells compromise the T cell response to new infections, but memory cells generated from aged naïve CD4 T cells also exhibit defective responses[24], and thymic atrophy is also associated with impaired negative selection and increased release of autoreactive T cells into the periphery and subsequent autoimmune disease[25, 26, 27, 28, 29, 30, 31, 32].

Although thymus dysfunction begins relatively early in life, a recent study demonstrated that it retains significant protective capacity in adults. When outcomes were compared between cardiac surgery patients who underwent complete thymectomy at the time of surgery and those in whom a thymic "remnant" was retained, complete thymectomy increased all-cause mortality, cancer risk, cancer severity, and autoimmune disease risk 5 years after surgery[33], strongly supporting the notion that increasing thymus function holds strong potential for significantly improving T cell function in older adults.

The thymus retains regenerative capacity with age[34, 35], and previous studies suggest that thymic regeneration increases immunity to microbial infections and tumor surveillance[36]. Approaches to induce thymus regeneration have so far only resulted in transient success, are limited by age and do not completely restore thymic function or transcriptional programs[37, 38, 39]. Improving our understanding of thymic growth and regeneration could inform better translational strategies for extending the healthspan. The most significant barrier to identifying effective approaches for thymus regeneration is a limited understanding of the mechanisms that regulate thymus growth. Although these mechanisms

are not fully resolved, it is clear that the primary targets of both age-induced atrophy and experimental thymic regeneration are stromal, rather than lymphoid cells[40, 41], particularly cortical stromal cells[42]. Stromal cells represent less than 1% of the total thymic cellularity[43] and their isolation requires enzymatic digestions known to induce important changes in their biology[44]. To overcome these barriers, we applied a computational deconvolution approach to estimate global stromal gene expression signatures[45, 46]. Application of this approach over the course of aging and experimentally induced thymus regeneration revealed that cTEC size and morphology are primary determinants of overall thymus size, and therefore new T cell generation, across the lifespan.

These analyses also suggested a critical role for mTOR signaling (through two distinct complexes) in regulating the size and morphology of cTECs[45], consistent with the observation that high dose rapamycin administration, which inhibits both mTORC1/2 activity[47], has been shown to decrease thymus size[48]. We found that the expression patterns of soluble ligands capable of activating the mTOR pathway were either absent or unchanged during aging and regeneration in cortical stromal cells, making autocrine signaling unlikely[45]. However, expression of known TEC regulator FGF21[49] was diminished with age, and dynamically regulated in medullary stromal cells during regeneration[45]. *Fgf21* expression has previously been reported in thymic stromal cells[49] and mTECs in particular[50], and expression of its obligate coreceptor βKlotho (*Klb*[51, 52]) has been reported in cTEC[49], but not in other thymic subsets[50]. Expression of *Fgf21*, but not *Klb,* declines with age in the thymus, and transgenic overexpression of *Fgf21* in the liver delays thymic atrophy in mice[49].

These findings led us to hypothesize that FGF21 expression by mTECs promotes direct or indirect paracrine activation of mTORC1/mTORC2 in cTECs to regulate cell proliferation, individual cell size, and morphology, thereby controlling overall thymus size. To test this hypothesis, we designed a knock-in mouse model in which overexpression of FGF21 is driven broadly in most mTECs. Here we report that paracrine FGF21 signaling activates temporally distinct patterns of mTORC1 and mTORC2 signaling in cTECs, which is sufficient to increase thymus size and function in aging mice, resulting in increased T cell responsiveness to influenza infection as well as decreases in indicators of

autoreactivity, relative to age-matched controls.

Results

Expression of *Fgf21* by mTECs declines with age

Because our previous studies indicated a role for *Fgf21* expressed by medullary stromal cells in the regulation of thymus growth[45], we sought to characterize the stromal cell subsets expressing *Fgf21* across the lifespan. Analysis of a previously published single-cell RNA-seq dataset[25] revealed that among the nine subsets of TECs identified, *Fgf21* expression was found at the highest levels in mature mTECs (*Aire*^{hi}, *Cd52*^{hi}), as well as proliferating TECs, which is a rarer population resembling mature mTECs (previously described as mTEC II (MHC-II^{+}, Ly6d^{-}))[53] seen predominantly in the early postnatal period[25, 54] (Fig. 1a). *Fgf21* expression in mature mTECs was highest during the early postnatal period and declined after 4 weeks of age, persisting at lower levels through 52 weeks (Fig. 1a). In contrast, *Fgf21* expression in proliferating TECs remained high through middle age. However, since the overall abundance of this population declined significantly following the postnatal period (Fig. 1b), the total amount of FGF21 produced by this subset of cells would be expected to decline during aging. *Fgf21* expression was detected at minimal levels in mature cTECs (*Prss*16^{hi}, *Cxcl12*^{hi}) throughout the first year, and in a small population of structural TEC (sTEC: *Cd177*^{hi}, *Car8*^{hi}) likely to be found in the medulla based on expression of *Enpp2*[55] (Fig. 1a-b). Thus, single-cell transcriptomic evidence confirmed mature mTECs as a primary source of *Fgf21* within the thymus, and also confirmed age-associated declines in *Fgf21* expression, consistent with previous reports[45, 49].

Identification of *Lpo* as a candidate mTEC gene

To begin to identify the role of mTEC-derived FGF21 in the regulation of thymus size, we designed a mouse model to drive gene expression broadly, but specifically, in mTECs in the thymus. Using the previously described transcriptional datasets[45], we applied a series of selection criteria to prioritize broadly expressed mTEC genes (Fig. 1c). The top candidate genes were ranked based on confidence

of medullary stromal expression and relative tissue specificity in a published database of gene expression across a broad range of tissue types (BioGPS GeneAtlas MOE430, gcrma). To avoid selecting Aire-dependent genes, which are expressed by only a subset of mTECs, typically at low levels, we excluded Aire-regulated genes using two previously published gene lists[56, 57]. Among the top candidate genes was *Lpo* (Lactoperoxidase), which was predicted to have highly specific expression in the thymic medullary stroma, lacrimal, and salivary glands. Immunofluorescence microscopy confirmed that within the thymus, LPO expression was preferentially expressed in the medulla, with a high degree of co-localization with TECs expressing the highest levels of EpCAM, which is characteristic of mTECs (Fig. 1d), and, importantly, remained highly expressed in the thymus at 12 months of age (Fig. 1d). Similar to *Fgf21*, *Lpo* expression was highest in mature mTECs and proliferating TECs and remained high during the first year of life[25] (Extended Data Fig. 1). To further confirm that *Lpo* expression was not Aire-dependent, we analyzed a previously published microarray database comparing gene expression between FACS-sorted wild-type and Aire-deficient mTECs[58], which revealed that expression of *Lpo* appears to be Aire-independent (Supplementary Table 1a). However, expression of *Lpo* was modestly but significantly lower in mTECs of *Fezf2*$^{-/-}$ mice[59] compared to wild-type mice, suggesting *Lpo* expression, or the population of cells expressing *Lpo*, may be partially regulated by Fezf2 (Supplementary Table 1b). Upon validation of *Lpo* as a candidate for driving gene expression broadly in most mTEC, we designed a bicistronic vector allowing for the insertion of *Fgf21* and mCherry cDNA at the end of Exon 13 of the *Lpo* gene by incorporating P2A and T2A sequences (Extended Data Fig. 2a, Fig. 1e). We then utilized CRISPR-Cas9 to generate founder mice expressing the Lpo-Fgf21-mCherry knock-in (KI) allele (Fig. 1e). Sanger sequencing and PCR verification confirmed expression of the knock-in mutation in founders (Extended Data Fig. 2b-c), which we subsequently backcrossed with C57BL/6 mice to create heterozygous LPO$^{FGF21/WT}$ and homozygous LPO$^{FGF21/FGF21}$ experimental mice. Unless otherwise indicated, heterozygous mice (LPO^{FGF21}) were used for experiments.

We first performed flow cytometric evaluation of mCherry reporter expression among thymic stromal subsets to confirm expression of the KI allele in mTEC subsets (Fig. 2a, Extended Data Fig. 3a). We

found mCherry to be expressed specifically in mTEC, and broadly among various mTEC subsets, including UEA1^{+} mTEC (CD45.2^{-}, EpCAM^{+}, Ly51^{-}, UEA1^{+}), mTEC^{lo} (CD45.2^{-}, EpCAM^{+}, Ly51^{-}, MHCII^{lo}, CD80^{lo}) and mTEC^{hi} (CD45.2^{-}, EpCAM^{+}, Ly51^{-}, MHCII^{hi}, CD80^{hi}) (Figure 2b). mCherry was not detected in cTEC (CD45.2^{-}, EpCAM^{+}, Ly51^{+}, UEA1^{-}), cDC (CD45.2^{+}, CD11c^{+}, B220^{-}), pDC (CD45.2^{+}, CD11c^{+}, B220^{+}), endothelial cell (EC) (CD45.2^{-}, EpCAM^{-}, CD31^{+}), pericyte (PC) (CD45.2^{-}, EpCAM^{-}, CD31^{-}, PDGFR$\alpha\beta^{+}$, CD146^{+}, gp38^{-}), or fibroblast (Fb) (CD45.2^{-}, EpCAM^{-}, CD31^{-}, PDGFR$\alpha\beta^{+}$, CD146^{-}, gp38^{+}) subsets (Fig. 2b), consistent with publicly available datasets[60]. Expression of mCherry ranged from 50-75% of all mTEC, and was detected in a proportion of all mTEC subsets evaluated (Fig. 2c). The frequency of mCherry positive cells was slightly diminished with age in most mTEC subsets in LPO^{FGF21} knock-in mice (Extended Data Fig. 3b), however the average mCherry MFI was generally maintained, except among mTEC^{lo} (Extended Data Fig. 3c). To further evaluate mCherry expression, we performed immunofluorescence microscopy. Thymic sections from 1-month-old LPO^{FGF21} and LPO^{WT} littermate controls were stained with fluorescent antibodies targeting K5, K8, DEC 205, Ly51, UEA1, and Aire. Co-localization with medullary markers K5, UEA1, and Aire, but not with cortical markers K8, DEC 205, and Ly51 indicated broad and specific medullary expression of the KI allele in the thymus (Fig. 2d, Extended Data Fig. 4a-e, Supplementary Fig. 1a-e).

To quantify gene expression in the LPO^{FGF21} KI thymus, we measured *Lpo*, *Fgf21*, and *mCherry* mRNA in FACS-sorted mTECs as well as whole salivary gland, liver, and lung tissue from 1-month-old LPO^{FGF21} and LPO^{WT} littermate controls (Extended Data Fig. 5a-c). We detected robust expression of *Lpo* in the salivary glands (maximally expressing tissue predicted by Biogps.org database) and mTEC of both LPO^{WT} and LPO^{FGF21} mice (Extended Data Fig. 5a), suggesting KI alleles do not disrupt *Lpo* expression. *Fgf21* was significantly increased and mCherry was robustly expressed in the salivary glands of LPO^{FGF21} mice (Extended Data Fig. 5b-c). These results were confirmed with immunofluorescence microscopy showing robust expression of LPO and mCherry in salivary gland epithelium of LPO^{FGF21} mice (Extended Data Fig. 4f). *Fgf21* expression was significantly increased, by

about 4-fold, in LPO^{FGF21} mTECs compared to LPO^{WT} littermate controls (Extended Data Fig. 5b-c). In the liver, *Fgf21* was expressed at similar levels in LPO^{WT} and LPO^{FGF21} mice, while *Lpo* and *mCherry* mRNA were undetectable (Extended Data Fig. 5a-c). Expression of *Lpo*, *Fgf21*, and *mCherry* were not detectable in the lungs of either LPO^{WT} or LPO^{FGF21} mice (Extended Data Fig. 5a-c). FGF21 can signal via FGFR1 or FGFR3 but requires the βKlotho co-receptor, and, expression of βKlotho by CD45^{-} thymic stromal cells has been shown to increase with aging[49]. To address which thymic stromal subtypes may express these co-receptors, we measured expression of *Klb*, *Fgfr1*, and *Fgfr3* in FACS-sorted thymic macrophages (CD19^{-}, CD11b^{+}, F4/80^{+}), fibroblasts (CD45^{-}, EpCAM^{-}, CD31^{-}, gp38^{+}), and mTECs (CD45^{-}, EpCAM^{+}, Ly51^{-}) from 6-month-old C57BL/6 mice (Extended Data Fig. 5d-f). *Klb* was undetectable in thymic fibroblasts and macrophages but was partially expressed in mTECs at levels similar to white adipose tissue and pancreas (Extended Data Fig. 5d). *Fgfr1* expression was significantly higher in mTECs and was detected at low levels in macrophages (Extended Data Fig. 5e). *Fgfr3* was expressed at about the same level as *Klb* in mTECs and was undetectable in macrophages and fibroblasts (Extended Data Fig. 5f). We were unable to purify cTECs in sufficient numbers to evaluate FGF21 receptor expression in this population by qRT-PCR. In agreement with Youm et. al.[61] these data suggest that mTECs and other thymic stromal cells not yet identified may respond to FGF21. mTEC-driven FGF21 overexpression did not increase circulating FGF21 levels, as serum levels of FGF21 did not significantly differ between age-matched LPO^{WT} and LPO^{FGF21} mice when measured in 1-month-old and 13-month-old mice (Extended Data Fig. 5g,i). While circulating FGF21 levels increased slightly with aging, consistent with previous reports[62], no differences were detected among age-matched LPO^{WT} and LPO^{FGF21} mice. However, whole thymus FGF21 production was found to be significantly higher in both young (1-month-old) and older (13-month-old) LPO^{FGF21} knock-in mice compared to LPO^{WT} age-matched controls when measured by ELISA (Extended Data Fig. 5h). Taken together, these results indicate faithful expression of the Lpo-Fgf21-mCherry knock-in allele in mTECs and in salivary gland.

FGF21 overexpression increases thymus size across the lifespan

To determine the effects of constitutive mTEC-mediated FGF21 overexpression on thymus size during aging, we compared thymus somatic index (thymus weight:body weight ratio) in LPO^{WT} and LPO^{FGF21} littermates from 1-14 months of age (Fig. 3a). While thymus size declined in both LPO^{WT} and LPO^{FGF21} mice with age, the thymus somatic index remained significantly increased in LPO^{FGF21} mice relative to age-matched controls (Fig. 3a). Body weights did not significantly differ up to 18-21 months in LPO^{WT} and LPO^{FGF21} mice (Extended Data Fig. 5i). Thymus cellularity was increased in both male and female LPO^{FGF21} mice at 1, 3, and 12-14 months of age relative to control littermates (Fig. 3b, Extended Data Fig. 6a), and the average thymus cellularity of 12-14-month-old LPO^{FGF21} KI mice was similar to that of 3-month-old LPO^{WT} littermates in males and females (Fig. 3b, Extended Data Fig. 6a). We next analyzed the thymic CD4/CD8 T cell subset frequencies and total numbers in 1-month- and 12-14-month-old LPO^{FGF21} mice. The relative frequency of each subset (DN, DP, $CD4^+$ SP, $CD8^+$ SP) did not significantly differ between LPO^{WT} and LPO^{FGF21} mice at any age tested (Fig. 3c, Extended Data Fig. 6b-c). The frequency of cTECs was increased in 1-month-old LPO^{FGF21} mice relative to controls, but was not significantly different in 12-14-month-old mice (Fig. 3c, Extended Data Fig. 6c). 12-14-month-old LPO^{FGF21} mice had increased total numbers of DN, DP and $CD4^+$ SP lymphocytes ($CD8^+$ SP numbers trended up but increase was not statistically significant), as well as increased cTECs and mTECs, highlighting the effect of FGF21 overexpression on preserving the total number of TEC as well as supporting lymphocyte development (Fig. 3d, Extended Data Fig. 6c). We observed no difference in proliferation or apoptosis (Extended Data Fig. 7a-d) in cTECs and mTECs of 3-month-old LPO^{WT} and LPO^{FGF21} mice, suggesting that the increased TEC numbers found in young LPO^{FGF21} mice relative to controls were maintained during aging without impacts on proliferation or survial at later ages.

Kinetics of mTORC1 and mTORC2 signaling in cTECs

Our prior work[45] and that of others[63] suggested mTOR complexes as potential downstream mediators of FGF21 signaling in cTECs, and transcriptional mTOR targets were dynamically regulated in cortical stroma upon castration-induced regeneration of the thymus[45]. To characterize changes in mTOR

pathway activation at the protein level, we first investigated changes in mTORC1/mTORC2 signaling during aging using antibodies measuring phosphorylation of p4E-BP1 and pAkt^{S473}, respectively, by flow cytometry[64] in cTECs, mTECs, and CD45^{+} lymphocytes from C57BL/6 mice (Fig. 4a-b). We first compared activation of p4E-BP1 and pAkt^{S473} in 3-week-old mice, representing a period of active thymus growth, and 6-month-old mice, representing a period of age-associated atrophy. We observed a significant age-associated decline in mTORC1 as well as mTORC2 activation in cTECs (Fig. 4a-b). We also observed a small but significant decline in p4E-BP1 and pAkt^{S473} levels in mTECs, but not in CD45^{+} lymphocytes (Fig. 4a-b). The high mTOR activity in young TEC followed by declines in aging are consistent with previous work indicating roles for mTOR signaling in TEC growth[65, 66, 67, 68]. We next evaluated the impact of mTEC-driven FGF21 overexpression on mTORC1/mTORC2 activity during aging. At 2.5 weeks of age, when the thymus is actively growing, LPO^{FGF21} KI cTECs in males and females showed evidence of significantly increased mTORC1, but not mTORC2 activity, compared to LPO^{WT} controls (Fig. 4c-d, Extended Data Fig. 8a-b). At 3 months of age, representing a shift from peak growth to a period of atrophy, LPO^{FGF21} mice had significantly increased pAkt^{S473}, but not p4E-BP1, levels (Fig. 4c-d, Extended Data Fig. 8a-b). This trend continued at 12 months of age, with mTORC2, but not mTORC1 activity significantly increased in cTECs of LPO^{FGF21} mice (Fig. 4c-d, Extended Data Fig. 8a-b). However, in mTECs there appeared to be only dynamic regulation of mTORC1, with increased p4E-BP1 in mTECs of 2.5-week-old LPO^{FGF21} mice, but not mTORC2, activity (Extended Data Fig. 8c-d). In CD45^{+} lymphocytes we observed no effect of LPO^{FGF21} KI allele expression on mTORC1/mTORC2 activity (Extended Data Fig. 8e-f), suggesting that FGF21 overexpression driven by mTECs signaled primarily in a paracrine manner to cTECs to affect mTORC1 and mTORC2 activation at distinct times during tissue growth and maintenance. The shift from increased mTORC1 to increased mTORC2 signaling during the transition from early thymus growth to later phases is consistent with our previous observation that expression of the mTORC1 regulator *Tsc1* is upregulated after the first few days of thymus growth during regeneration[45]. To test whether Tsc1 expression was similarly upregulated during later phases of postnatal thymic growth, we compared TSC1 expression in cTECs of 3-week-old, 6-week-old, and 4-month-old LPO^{WT} mice by

flow cytometry. Consistent with the kinetics of thymus growth during regeneration, we found that TSC1 expression was low at early growth stages, and steadily increased during aging (Fig. 4e). To further understand the kinetics of mTOR/TSC1 signaling in the cortical stroma in the actively growing/regenerated thymus, we utilized a previously published stromal transcriptome database collected during thymic regeneration to evaluate expression of a manually curated set of genes that are targets of transcription factors (TFs) known to be regulated by mTORC1 (reviewed in[69, 70]). These included targets of TFs positively regulated by mTORC1, sterol-regulatory-element-binding proteins (SREBPs), *Fasn* and *Acaca* (AKA *Acc1*) in the same published dataset described above described above[45] (Fig. 4f, green). The expression of these genes increases during early stages of thymic regrowth (peaking around day 10 of regeneration), consistent with positive regulation by mTORC1. Also consistent with increased mTORC1 activity during early phases of thymic regrowth, expression of target genes regulated by a TF inhibited by mTORC1, transcription factor EB (TFEB), *Sqstm1* and *Lamp1*, declines during early phases of thymic regrowth (Fig. 4f, red). Repression of genes important for lipid oxidation (*Sqstm1, Lamp1*), in favor of those involved in lipid biogenesis (*Fasn*, *Acaca*), is consistent with the notion that thymic regrowth requires re-extension of cTEC cellular projections, which would require anabolic metabolism increasing lipid incorporation into extending cellular membranes. Fewer transcriptional targets of mTORC2 signaling have been identified, however, recent work identified several members of the Hedgehog pathway as targets positively regulated at the transcriptional level by mTORC2 activity[71] . Of those identified in this study, *Gli3* was included in our high-confidence cortical stromal gene list (Fig. 4f, blue circles). Consistent with the notion that mTORC1 activity is increased early during cTEC growth phases, followed by Tsc1-mediated down-regulation that would favor mTORC2 activity promoting cytoskeletal rearrangements and maintenance of cTEC labyrinth morphology, we find that mTORC1-dependent changes in gene expression begin to revert after about day 10 during regeneration. Conversely, we find that expression of the mTORC2 target Gli3 begins to increase around day 10 (Fig. 4f). Together, these results are consistent with the hypothesis that FGF21 signaling predominantly mediates mTORC1 signaling in cTECs during early phases of thymus growth, while mTORC2-mediated signaling predominates at later stages. However,

it is likely that other upstream ligands or metabolites also contribute to changes in mTORC1/2 signaling across the lifespan.

We next examined whether pharmacological mTOR inhibition mitigates the impact of FGF21 overexpression on thymus size, $CD4^+CD8^+$ DP thymocyte number, and mTOR activity in cTECs. 3-week-old LPO^{WT} and LPO^{FGF21} littermates were injected with 4 mg/kg rapamycin or vehicle via intraperitoneal injection every other day for 2 weeks, as previously described[72, 73] (Fig. 5a). After two weeks of treatment, rapamycin induced a significant decline in the thymus somatic index in both LPO^{WT} and LPO^{FGF21} mice (Fig. 5b). Total thymus cellularity was also significantly reduced in rapamycin-treated LPO^{WT} and LPO^{FGF21} mice (Fig. 5c), abrogating the effects of FGF21-mediated increases in thymus cellularity. We observed a significant decrease in the frequency of $CD4^+CD8^+$ DP lymphocytes and a significant increase in the frequency of $CD4^-CD8^-$ DN lymphocytes of rapamycin-treated LPO^{WT} and LPO^{FGF21} mice (Fig. 5c, top panel), consistent with previous studies[74, 75]. In LPO^{FGF21} knock-in, but not LPO^{WT} mice, we also observed a significant increase in the frequency of $CD8^+$ SP lymphocytes (Fig. 5c, top panel). However, when we compared the total cell number of each of these thymocyte subsets, rapamycin only induced a significant decrease in the total number of $CD4^+CD8^+$ DP lymphocytes, and did so in both LPO^{WT} and LPO^{FGF21} mice (Fig. 5c, bottom panel). The total number of DP lymphocytes were reduced to similar levels in LPO^{WT} and LPO^{FGF21} rapamycin-treated mice, despite LPO^{FGF21} vehicle-treated mice having a significantly higher number of DP lymphocytes compared to LPO^{WT} vehicle-treated mice (consistent with Fig. 3c). We also observed a decreasing trend in the total number of $CD4^+$ SP lymphocytes in rapamycin-treated LPO^{FGF21} mice (Fig. 5c), which may reflect increased autophagy following relief of mTORC1 inhibition, leading to more MHCII-mediated negative selection of $CD4^+$ SP lymphocytes relative to $CD8^+$ SP lymphocytes[76].

When we compared mTORC1/mTORC2 signaling in cTECs, mTECs, and lymphocytes in vehicle-treated and rapamycin-treated LPO^{WT} and LPO^{FGF21} mice (Fig. 5d-e), we found that rapamycin treatment induced a significant decrease in pS6 (indicator of mTORC1 activity[77]) signaling in cTECs, mTECs, and lymphocytes of LPO^{FGF21} mice (Fig. 5e). Rapamycin treatment promoted a trend toward

decreased pS6 levels in cTECs of LPO^{WT} mice but was not statistically significant, while pS6 significantly declined in mTECs and $CD45^+$ lymphocytes of LPO^{WT} mice (Fig. 5e). $pAkt^{S473}$ only decreased in rapamycin-treated cTECs of LPO^{FGF21} mice (Fig. 5f). Rapamycin treatment has direct negative effects on DP thymocyte survival[74, 75], but our data are nonetheless consistent with the hypothesis that the effects of FGF21 overexpression on thymus size are mediated through mTOR pathway activation in TECs.

FGF21 overexpression improves T cell responses to influenza

Based on the observation that FGF21 overexpression increased thymus size, we next evaluated peripheral T cell changes induced by mTEC-driven FGF21 overexpression. We first compared the ratio of naïve ($CD62L^+$, $CD44^-$): memory ($CD62L^+$, $CD44^+$) $CD8^+$ T cells in the spleens of 2-month-old and 12-month-old LPO^{WT} and LPO^{FGF21} KI mice (Fig. 6a). While we found no significant difference in the $CD8^+$ naïve:memory ratio of 2-month-old mice, we found a significant increase in 12-month-old LPO^{FGF21} mice compared to LPO^{WT} controls (Fig. 6b), suggesting improved export of naïve T cells into the periphery of aged LPO^{FGF21} mice. We also found similar increases in the naïve:memory ratio of $CD4^+$ splenocytes in aged LPO^{FGF21} mice, consistent with increased export of thymic $CD4^+$ SP T cells seen during aging (Fig. 3d, 6d, Extended Data Fig. 6c).

The decline in T cell immunity due to decreased thymic output during aging is thought to narrow the TCR repertoire, for instance by diminishing the frequency of T cells specific for some flu epitopes[78, 79], which can be rescued upon thymus regeneration[36]. To test the functional capacity of peripheral T cells in LPO^{FGF21} mice, we challenged 12-month-old LPO^{WT} and LPO^{FGF21} mice with 10^3 PFU of influenza A (IAV) X31 via intranasal infection (Fig. 6e), and monitored changes in body weight over the course of ten days. X31-infected LPO^{FGF21} mice lost significantly less weight relative to control littermates (Fig. 6f). Similarly, when older 18-month-old LPO^{FGF21} mice were challenged with IAV PR8 (10^3 PFU), we observed a significant reduction in the amount of body weight lost compared to PR8-infected age-matched LPO^{WT} controls at 7 dpi, suggesting improved control of infection (Extended

Data Fig. 9). Because short-term stressful stimuli such as infection induce rapid thymic atrophy[80, 81, 82], we compared total thymus cellularity at 10 dpi (Fig. 6g). We found that infected aged LPO^{FGF21} mice had significantly greater thymus cellularity than infected LPO^{WT} controls (Fig. 6g). Infected LPO^{FGF21} mice had significantly decreased influenza mRNA in the lung compared to infected LPO^{WT} mice at 10 dpi, suggesting improved viral clearance (Fig. 6h). At 10 dpi bronchiolar lavage (BAL), spleen, and mediastinal lymph nodes (MLN) were also harvested to measure the frequency and total number of influenza-specific $CD8^+$ T cells via $NP_{366-374}$ tetramer staining, as previously described[32] (Fig. 6i-j). Both the frequency and total number of NP-specific $CD8^+$ T cells were significantly increased in the BAL of infected LPO^{FGF21} mice relative to controls, while no difference was observed in the spleen or MLNs of infected mice (Fig. 6i-j). These results suggest that FGF21 overexpression increases the number of influenza-specific T cells available to respond to infection in the BAL. Taken together, these observations suggest that FGF21 overexpression in mTECs mitigates waning naïve T cell frequency and T cell responsiveness to influenza infection in older mice.

The observations that aged LPO^{FGF21} mice have increased export of naïve $CD4^+$ and $CD8^+$ T cells, as well as improved T cell responsiveness to viral infection, led us to consider the impact of increased thymic FGF21 signaling on TCR repertoire diversity. Aging induces monoclonal and oligoclonal expansion of CD8 T cells, resulting in dampened immune responses to infection[83, 84, 85]. To address the impact of increased intrathymic FGF21 signaling on CD8 TCR repertoire diversity during aging, we measured the frequency of $V\beta2^+$, $V\beta7^+$, $V\beta8^+$, and $V\beta11^+$ CD8 T cells in peripheral blood lymphocytes of 2-month-old and 12-month-old LPO^{WT} and LPO^{FGF21} mice (Extended Data Fig. 10a). Though previous studies demonstrated expansion of $V\beta8^+$ and $V\beta11^+$ CD8 T cells >15-20 months of age[83], we found no significant difference in Vβ frequency between LPO^{WT} and LPO^{FGF21} mice during the first year of life (Extended Data Fig. 10b-e). These data suggest that mTEC-driven FGF21 overexpression may not impact age-associated CD8 T cell clonal expansion. However, differences may not be apparent until later in life[83], and this approach may not be sensitive enough detect subtle differences.

FGF21 overexpression mitigates impairment of T cell tolerance

With the observation that FGF21 overexpression improved the age-associated decline in naïve T cells and improved outcomes to influenza infection, we next evaluated age-associated declines in clonal deletion among signaled ($CD5^+$ $TCR\beta^+$) thymocytes using flow cytometry[86], as previously reported[32, 87] (Fig. 7a). We compared both early clonal deletion, occurring among $CCR7^-$ signaled thymocytes, and later clonal deletion occurring among $CCR7^+$ thymocytes, in 2-month-old and 12-month-old LPO^{WT} and $LPO^{FGF21/FGF21}$ homozygous KI mice (Fig. 7a). As we and others have previously reported[25, 31, 32, 87], we observed an age-associated decline in the frequency of both early and late clonally deleted (cleaved caspase 3^+) thymocytes in LPO^{WT} mice (Fig. 7b). Clonal deletion of early and late signaled thymocytes were both significantly higher in the LPO^{FGF21} mice at both timepoints compared to LPO^{WT} controls (Fig. 7b). Surprisingly, while we observed an age-associated decline in the clonal deletion of late ($CCR7^+$) thymocytes in LPO^{FGF21}mice (though this was less pronounced than the decline in LPO^{WT} mice), early ($CCR7^-$) clonal deletion was preserved at the level of young mice in 12-month-old LPO^{FGF21} mice (Fig. 7b), suggesting potential indirect effects of FGF21-mediated paracrine signaling to preserve earlier stages of clonal deletion.

We next evaluated 12-month-old LPO^{FGF21} mice for the presence of indicators of peripheral autoimmunity. LPO^{FGF21} mice had a lower frequency of antinuclear antibodies (ANAs) in the serum, with only 25% of KI animals testing positive for the presence of antinuclear IgG (compared to 75% of LPO^{WT} animals) (Fig. 7d). We further investigated the impact of FGF21 overexpression on development of peripheral autoimmunity by evaluating lung, liver, and salivary gland tissue from 12-month-old LPO^{FGF21} mice for the presence of inflammatory lymphocytic infiltrates (defined as >20 lymphocytes per foci). LPO^{FGF21} mice had decreased incidence of lymphocytic infiltrates in the liver and salivary gland, while incidence of infiltrates in the lung generally did not differ from LPO^{WT} mice (Fig. 7e). Since LPO is expressed in salivary gland, it is possible that changes in local salivary gland expression of LPO may contribute to differences in lymphocytic infiltrates in this tissue.

To address whether these observed differences in peripheral autoreactivity could be partially explained by differences in Treg frequencies, we measured the frequency of $CD4^+$ Tregs ($CD25^+$ $Foxp3^+$) in splenocytes from 2-month-old and 12-month-old LPO^{WT} and LPO^{FGF21} mice (Fig. 7f). Constistent with previous work[88, 89, 90], we observed an age-associated increase in $CD4^+$ Tregs in both LPO^{WT} and LPO^{FGF21} mice as well as an age-related increase in both genotypes of $CD25^{lo}$ $CD4^+$ Tregs (Fig. 7g). In both groups of aged animals, we noted an apparent increase in the population of, which is also consistent with previous reports[90]. Notably, 12-month-old LPO^{FGF21} mice had a higher frequency of $CD4^+$ Tregs compared to age-matched LPO^{WT} controls (Fig. 7g). Expression of the transcription factor Helios has been used to distinguish thymic-derived tTregs from peripherally-derived pTregs[91, 92]. Consistent with reduced thymic output in the aged thymus, we observed a decrease in the frequency of $Helios^+$ Tregs and an increase in the frequency of $Helios^-$ Tregs in splenocytes of 12-month-old LPO^{WT} mice, while the frequencies of $Helios^+$/$Helios^-$ CD4 Tregs were not significantly different between 1-month-old and 12-month-old LPO^{FGF21} mice (Fig. 7h-i). These results, together with our peripheral naïve T cell and infection data, support the conclusion that mTEC-derived FGF21 overexpression improves thymus function in older mice to preserve T cell output while maintaining both generation of Tregs and negative selection of autoreactive T cells during aging.

Paracrine FGF21 signaling increases cTEC size during aging

cTECs form networks of finely branched processes which create the structural niches required for T lymphocyte development, and limit the overall size of the thymus[93]. We have previously demonstrated that aging is associated with a marked contraction of the cortical compartment, predominantly resulting from contraction of cTEC size and cortical projections[45]. To address whether paracrine FGF21 signaling to cTECs would protect cell size during aging, we compared cTEC size and morphology between 1-month-old and 6-month-old LPO^{WT} and LPO^{FGF21} KI mice crossed with $FoxN1^{Cre}$ $R26^{Confetti}$ reporter mice, which allows for labeling of individual TEC[45, 94]. Qualitative analysis of cTEC morphology in 3D projections from 60 μm optical stacks revealed a significant contracture of cTEC cell size in 6-month-old LPO^{WT} mice, with the most striking changes occurring in the subcapsular

zone as we have previously reported[45] (Fig. 8a-b, Supplementary Videos 1-2). In contrast, cTECs in 6-month-old LPO^{FGF21} mice retained more of their labyrinth morphology, more closely resembling that seen in 1-month-old mice (Fig. 8c-d, Supplementary Videos 3-4). Quantification of cTEC cell area revealed that while aging induced a significant reduction in average cTEC size in 6-month-old FoxN1^{Cre} R26^{Confetti} LPO^{WT} thymi, age-matched FoxN1^{Cre} R26^{Confetti} LPO^{FGF21} thymi were protected from decreases in cTEC size (Fig. 8e). These results, in agreement with our observed increased activation of pAkt^{S473} in cTECs of aged LPO^{FGF21} KI mice (Fig. 4d, Extended Data Fig. 8b), indicate a potential role for FGF21-mediated activation of mTORC2 in maintenance of cTEC cell morphology and overall size.

Discussion

Thymus size is dynamic over the lifespan, and is regulated by both reversible responses to stimuli including steroid hormones, infections and stressors, as well as progressive age-associated factors[95, 96, 97, 98]. In this study, we found that FGF21 overexpression in the thymus resulted in a larger thymus size early in life, which persisted during aging. This is consistent with the view that common signaling[99], environmental[100], and/or epigenetic[101, 102] mechanisms may regulate both developmental processes and aging outcomes. For instance, rapamycin treatment restricted to developmental windows extends lifespan in crustaceans, flies, and mice[103, 104], and larval crowding extends lifespan in flies[105, 106, 107, 108, 109], as does litter crowding in mice[110]. Similarly, short exposure to growth hormone during early postnatal periods restricts lifespan in long-lived Ames dwarf mice[111]. Together, these findings support the notion that developmental processes, even during the earliest periods in life, have functional consequences on the regulation of lifespan and healthspan. Given that the thymus begins to atrophy relatively early in life, it is possible that the thymus may be especially sensitive to such developmental effects on peak organ size and subsequent age-associated declines in size and function. Therefore, the increased thymus cellularity we find in older LPO^{FGF21} mice may result strictly from increased FGF21 activity during thymus development, during later periods, or both. Future studies designed to modulate FGF21 and mTOR signaling at distinct periods in the lifespan using

inducible, tissue-specific genetically modified mouse models will be required to distinguish these possibilities.

Although the steady state size of the thymus progressively declines with age, even that can be temporarily reversed in all tested species, including mice, non-human primates and humans (reviewed in[112]). Great progress has been made toward regeneration of thymus function in otherwise healthy aging adults[38, 113] and after exogenous insults, such as radiation[114, 115, 116, 117], but long-term, durable regeneration remains to be achieved. Notably, a population of "age-associated" TECs (aaTECs) linked with defective recovery of thymus cellularity following sublethal total body irradiation has recently been described, and have been linked with reduced expression of epithelial regenerative factors following acute injury (including *Fgf21*), presenting further barriers to reconstituting thymic function[118].

The transient nature of regeneration after castration is consistent with the fact that the gene expression signature of cortical stromal cells at the peak of regeneration is largely unchanged relative to the atrophied state[42], and with work demonstrating that accumulation of relatively large amounts of oxidative damage early in life in cTECs occurs as a result of the naturally low levels of the hydrogen peroxide quenching enzyme catalase[119] that are necessary to drive the conspicuously high levels of basal autophagy that is required for antigen presentation and induction of T cell tolerance[76, 87].

Together, these observations suggest that an optimal approach for durable regeneration may require protection from oxidative damage and sustained growth factor signaling to cTECs. Here we report that sustained paracrine FGF21 signaling does indeed partially mitigate atrophy and sequela (Fig. 3a-d, Fig. 6a-b). The kinetics of mTORC1/2 signaling and TSC1 expression in cTECs are consistent with a role for mTORC1 in regulating cell proliferation during early phases of thymus growth in young animals, followed by a shift toward mTORC2 activity during the steady state, and then declines in both FGF21 and mTOR signaling during atrophy (Fig. 4c-e; Extended Data Fig. 8a-b). Indeed, though mTORC1 signaling promotes cell growth, a TSC1-mediated shift away from mTORC1-mediated repression of autophagy has been shown to be important for TEC survival and function[120]. Notably,

FGF21 overexpression, unlike antioxidant overexpression[87], was protective against indicators of peripheral autoimmunity (Fig. 7b-e). Supporting a role for mTORC2 in preserving cellular morphology in cTECs during later stages of thymus maintenance, paracrine FGF21 also promoted increased cTEC cell size during aging (Fig. 8c-e). Together, the observations that overexpression of FGF21 increased individual cTEC size and early (cortical) T cell progenitor number, but not cTEC number, in older mice (consistent with Youm et. al.[61]), suggest that individual cTEC size is a key regulator of the number of niches available for T cell progenitors, and therefore overall thymus size. Because FGF21 is not a mitogen and has a strong safety profile[121, 122], it may represent an ideal candidate for meeting the growth signal criterion described above. Thus, an optimal approach for durable and safe thymus regeneration in adults may involve a combination of sustained FGF21 signaling, distinct periods of selective mTORC1/mTORC2 stimulation, and appropriate strategies for reducing oxidative damage in stromal cells.

Additionally, in this study we report the validation of Lactoperoxidase (*Lpo*) as a broadly expressed mTEC gene (Fig. 1d, 2b-d, Extended Data Fig. 1, 4a-e, 5a). While *Lpo* expression is not predicted to be Aire-dependent, its expression may be partially regulated by Fezf2, as evidenced by comparing *Lpo* expression between wild-type and Fezf2$^{-/-}$ mTECs in a previously published microarray dataset[59] (Supplementary Table 1b). Outside the thymus, *Lpo* is highly expressed in secretory structures including the salivary and lacrimal glands. While the physiological function of Lactoperoxidase in the thymus is currently unclear, it is known to oxidize thiocyanate ions to neutralize thiols produced by foreign microbes in the saliva, tears, and milk[123, 124, 125]. Emerging evidence supports the importance of maintaining an environment of low-grade sterile inflammation in the thymic medulla to promote self-tolerance, potentially through expression of type II and III interferons[126, 127]. Since inflammation is associated with increased oxidative stress, it is tempting to speculate that LPO's oxidizing activity may be beneficial for self-tolerance induction through the generation of oxidized self-peptides, as a mimic of oxidation events that may occur in the periphery during inflammation. In support of this concept, a study characterizing germline *Lpo* knock-out mice revealed widespread organ autoimmunity and

488 systemic inflammation[128]. Thus, *Lpo* expression in the thymus medulla may promote antimicrobial
489 defenses and/or promote an oxidative environment to allow induction of tolerance to oxidized self-
490 peptides.

491 Limitations of the study

492 Due to the direct effects of rapamycin on lymphocytes, it is difficult to directly assess the effects of
493 pharmacological mTORC1/mTORC2 inhibition on thymic stromal cell function. Similarly, it is not yet
494 clear whether FGF21 mediates changes in mTOR signaling in cTECs directly or indirectly. Future
495 studies incorporating cTEC-specific and mTEC-specific gene ablation or overexpression will be
496 required to more comprehensively define the cellular and molecular mechanisms regulating paracrine
497 FGF21 signaling in the thymus. Further studies will also be required to determine the downstream
498 effects of FGF21 signaling on cTEC cytoskeleton organization and proliferation. These are important
499 considerations, as age-associated contraction of the cortical epithelium would be expected to reduce
500 the capacity of the thymus to support selection of developing T cells[37,93]. Importantly, it also remains
501 to be seen whether increased thymic FGF21 expression has the capacity to reverse thymic atrophy
502 after it has already occurred in aged animals.

503 **Methods**

504 **Mice**

505 C57BL/6 (JAX: 000664) mice were purchased from The Jackson Laboratory (Bar Harbor, ME, USA)
506 at 4-6 weeks of age and subsequently used as breeders. Offspring were subsequently used for
507 experiments between 3 weeks-12 months of age. Sanger sequence-verified LPO^{FGF21} knock-in
508 founders were paired with C57BL/6 mice as breeders to generate $LPO^{FGF21/WT}$ heterozygous or
509 $LPO^{FGF21/FGF21}$ homozygous knock-in (KI) mice for experiments. Non-KI littermate controls were used
510 as WT controls. Mouse genotypes were determined using real time PCR with specific probes designed
511 for the LPO^{FGF21} knock-in mutation (Transnetyx, Cordova, TN). Male and female LPO^{WT} and LPO^{FGF21}
512 KI mice between 2.5 weeks-14 months of age were used for experiments. All mice used in

experiments were bred and maintained at The University of Texas Health Science Center at San Antonio animal facility under specific pathogen free conditions. Mice were kept with a 14 hour-light/10 hour-dark cycle (7 a.m. to 9 p.m.), and all mice were provided with food and water ad libitum. Mice were housed at a daily temperature of 75°F (with daily temperature difference +/-3 °F); and relative humidity was maintained between 30–70%. Animal studies and all procedures were approved by the Institutional Animal Care and Use Committee, under protocol number 20190095AR.

Generation of LPO^{FGF21} knock-in mice

Guide RNAs targeting *Lpo* gene stop codon at Exon 13 was identified utilizing CRISPOR.Tefor.net guide RNA search tool. Double Strand Break (DSB) of the crRNA, ACCATGGACATGTTCGATGT, was located 29bp from the foreign DNA Knock-In locus before the stop codon. The plasmid donor DNA was synthesized from GenScript (Piscataway, NJ); 1,443 base pair foreign DNA composed of T2A-mCherry-P2A-Fgf21 cDNA, flanked with 700bp 5' Homology Arm and 702bp 3' Homology Arm was cloned into pUC-57 backbone plasmid. PAM sequence was modified from AGG to AGa in donor DNA to silence Cas9 activity in it. sgRNAs (32ng/μl), donor DNA (15ng/μl), and eSpCas9 Nuclease (50ng/μl) were mixed in injection buffer (10mM Tris-NaCl, 0.25mM EDTA), and incubated at room temperature for 20 minutes before zygote microinjection session. sgRNAs were synthesized from Synthego (sgRNA with chemical modification), and eSpCas9 was purchased from Millipore-Sigma. PCR verification was performed to confirm successful knock-in mutation insertion in Sanger sequence-verified founders.

Quantification of *Fgf21* and *Lpo* expression in TEC subsets

Fgf21 and *Lpo* expression were quantified in 9 TEC populations described in a previously published single-cell transcriptome profiling dataset (ArrayExpress, E-MTAB-8560)[25]. scRNA-seq data obtained from the dataset (relative *Fgf21*/*Lpo* expression, TEC population frequencies from 1-52 weeks) were analyzed using the Seurat package in R.

Analysis of *Lpo* regulation expression by Aire and Fezf2

Regulation of thymic *Lpo* expression by Aire and Fezf2 was studied by measuring the log2 fold-change in *Lpo* expression between FACS-sorted mTECs of wild-type mice compared with *Aire*$^{-/-}$ and *Fezf2*$^{-/-}$ mice using two previously published microarray datasets (Aire$^{-/-}$: GSE:14365[58], Fezf2$^{-/-}$: GSE:69105[59]). The datasets indicated were analyzed using the GEO2R R script with default of options and all available replicates.

Stromal cell isolation

For thymic stromal cell isolation, thymi were harvested and minced into small pieces with scissors. Fragments were passed several times through a P1000 pipette. Thymus pieces were allowed to settle, after which the supernatant containing lymphoid cells was removed. The remaining fragments were digested with 0.125% collagenase D (Roche) for 10 minutes at 37°C. Three additional rounds of mechanical mixing, sedimentation, and removing lymphoid cells were performed, followed by a final digestion in 0.05% trypsin (Sigma). After the final digestion, cells were washed and pelleted by centrifugation (440 x g), then resuspended in FACS buffer (HBSS, 5% FBS, 0.05% DNAse) containing a cocktail of fluorescent antibodies recognizing Alexa 700-conjugated anti-CD45.2 (Ly-5.2) (Clone 104; Biolegend; 1:150 dilution), PECy-7-conjugated anti-EpCAM (CD326) (Clone G8.8; Biolegend; 1:600 dilution), and biotinylated anti-Ly-51 (Clone 6C3; Biolegend; 1:100 dilution)/PerCPCy5.5-conjugated streptavidin (Biolegend; 1:500 dilution). For dendritic cell isolation, after the final digestion, all the collected lymphoid cells and stromal cells were combined in one tube, washed, pelleted by centrifugation, and then stained with PerCPCy5.5-conjugated anti-CD45.2 (Clone 30-F-11; eBioscience; 1:200 dilution), APC-conjugated anti-CD11c (Clone HL3; BD Pharmingen; 1:150 dilutoin), FITC-conjugated anti-B220 (Clone RA3-6B2; Biolegend; 1:400 dilution), and PECy7-conjugated anti-EpCAM. For endothelial and mesenchymal (pericyte, fibroblast) cell isolation, stromal cells were stained with biotin-labeled anti-PDGFRα and anti-PDGFRβ (Clones APA5, APB5; Biolegend; 1:100 dilution), followed by incubation with a cocktail containing BV650-conjugated

Streptavidin (Biolegend; 1:500 dilution), FITC-conjugated anti-CD31 (Clone W18222B; Biolegend; 1:300 dilution), APC-conjugated CD146 (Clone ME-9F1; Biolegend; 1:150 dilution), PE-conjugated gp38 (Clone 8.1.1; Biolegend; 1:200 dilution), Alexa 700-conjugated CD45.2, and PE-Cy7-conjugated anti-CD326. Dead and/or dying cells were excluded by DAPI staining (0.1 μg/ml final concentration). For intracellular flow cytometry experiments, cells were stained with Zombie Violet viability dye (Biolegend #423113; 1:1000 dilution), then subsequently fixed and permeabilized using BD Cytofix/Cytoperm kit. Fixed and permeabilized cells were then stained with a cocktail of fluorescent antibodies recognizing APC-conjugated anti-Phospho-Akt^{S473} (Cell Signaling Technology #11962; dilution 1:50), PE-conjugated anti-Phospho-4EBP1$^{T36/45}$ (Clone V3NTY24; eBioscience; dilution 1:30), and PE-conjugated anti-Phospho-S6$^{S235/236}$ (Clone cupk43k; eBioscience); dilution 1:30). To measure TSC1 expression, fixed and permeabilized cells were incubated with pure anti-TSC1 (Clone A6F1; Invitrogen; dilution 1:200), followed by secondary staining with FITC-conjugated Goat Anti-Mouse IgG (Jackson #115-095-146; dilution 1:200). Flow cytometry analysis was performed on the Cytek Aurora spectral flow cytometer running SpectroFlo v3.3.0. Experiments were analyzed using FlowJo software (v10.9).

TEC proliferation/apoptosis

To measure the frequency of TECs undergoing apoptosis and/or proliferation, thymic stromal cells were enriched with collagenase as described above. Following surface staining, samples were washed with annexin binding buffer containing 10 mM HEPES, 140 mM NaCl, and 2.5 mM CaCl2 (pH 7.4), then incubated with APC-conjugated Annexin V (Invitrogen, catalog no. A35110; dilution 1:30) at room temperature for 10 minutes. Cells were washed with binding buffer and resuspended with Foxp3 Fixation/Permeabilization buffer (eBioscience, catalog no. 00-5523-00). After being fixed for 30 minutes on ice, samples were washed with permeabilization buffer, followed by incubation with FITC-conjugated anti-Ki67 (Clone 11F6, Biolegend; dilution 1:200) at room temperature for 30 minutes. Apoptotic cells were distinguished from dead cells via staining with LIVE/DEAD Blue (Invitrogen, catalog no. L23105; dilution 1:1000) prior to fixation/permeabilization.

Thymocyte subset isolation

Thymocyte CD4/CD8 populations were stained by preparing single-cell suspensions from whole thymi crushed against a mesh filter and subsequently filtered. 5 million cells per sample were stained with a cocktail of fluorescent antibodies containing APC-Cy7-conjugated anti-CD4 (Clone RM4-5; Biolegend; dilution 1:250) and BUV 395-conjugated anti-CD8 (Clone 53-6.7; BD Biosciences; dilution 1:250). DAPI staining was used to exclude dead/dying cells. Flow cytometry analysis was performed on the Cytek Aurora spectral flow cytometer running SpectroFlo v3.3.0. Experiments were analyzed using FlowJo software (v10.9).

TCR Vβ staining

To measure CD8 TCR repertoire diversity, peripheral blood lymphocytes were obtained from 2-month-old and 12-month-old mice. Briefly, blood was obtained via cardiac puncture and collected into 1.5 mL microcentrifuge tubes containing 50 µL EDTA (pH 8.0) kept on ice to prevent clotting. Blood samples were then transferred to a 15 mL conical tube and red blood cell lysis was performed with ACK lysis buffer. To measure the frequency of $V\beta2^+$, $V\beta7^+$, $V\beta8^+$, and $V\beta11^+$ CD8 T cells, samples were incubated with a cocktail of fluorescent antibodies containing APC-Cy7-conjugated anti-CD4, BUV395-conjugated anti-CD8, PE-conjugated anti-TCR Vβ2 (Clone B20.6; BD Biolegend; dilution 1:200), FITC-conjugated anti-TCR Vβ7 (Clone TR310; Biolegend; dilution 1:100), BV510-conjugated anti-TCR Vβ8 (Clone F23.1; BD Biosciences; dilution 1:200), and BV650-conjugated anti-TCR Vβ11 (Clone RR3-15; BD Biosciences; dilution 1:200). DAPI staining was used to exclude dead/dying cells prior to performing flow cytometry analysis.

Treg analysis

To measure the frequency of peripheral $CD4^+$ Tregs, single-cell suspensions were prepared from spleens harvested from 2-month-old and 12-month-old LPO^{WT} and LPO^{FGF21} mice. Briefly, after removing red blood cells with ACK lysis buffer, approximately $5x10^6$ splenocytes were incubated with a cocktail of fluorescent antibodies containing APC-Cy-7-conjugated anti-CD4, BUV 395-conjugated

anti-CD8, PE-conjugated anti-CD25 (Clone PC61; BD Biosciences; dilution 1:200), and BV650-conjugated anti-CD44 (Clone IM7; Biolegend; dilution 1:200). Samples were then washed and incubated with the Foxp3 Fixation/Permeabilization buffer described above. Following fixation and permeabilization, samples were incubated with PE-Cy7-conjugated anti-Foxp3 (Clone FJK-16s; eBioscience; dilution 1:250) and FITC-conjugated anti-Helios (Clone 22F6; Invitrogen; dilution 1:250). Flow cytometry analysis was performed on the Cytek Aurora spectral flow cytometer running SpectroFlo v3.3.0. Experiments were subsequently analyzed using FlowJo software (v10.9).

Gene expression qRT-PCR

Following enrichment of thymic stromal subsets with collagenase as described above, single-cell suspensions were enriched for mTECs by staining with FITC-conjugated anti-CD45.2 (Clone 104; Biolegend; dilution 1:300), PE-Cy7-conjugated anti-EpCAM, and A647-conjugated anti-Ly51 (Clone 6C3; Biolegend; dilution 1:100). To enrich for thymic macrophages, single-cell suspensions were stained with APC-conjugated anti-CD19 (Clone 6D5; Biolegend; dilution 1:200), FITC-conjugated anti-CD11b (Clone M1/70; Biolegend; dilution 1:500), and PE-conjugated anti-F4/80 (Clone BM8; Biolegend; dilution 1:200). To enrich for thymic fibroblasts, single cell suspensions were stained with APC-conjugated anti-CD45.2 (Clone 104; Biolegend; dilution 1:150), PE-Cy7-conjugated anti-EpCAM, FITC-conjugated anti-CD31 (Clone MEC13.3; Biolegend); dilution 1:200, and PE-conjugated anti-gp38 (Clone 8.1.1; Biolegend; dilution 1:200). Thymoyte subsets ($CD4^+$ SP, $CD8^+$ SP, $CD4^+$ $CD8^+$ DP, and $CD4^-$ $CD8^-$ DN) were isolated by staining with FITC-conjugated anti-CD8 (Clone H35-17.2; Invitrogen; dilution 1:200) and PE-conjugated anti-CD4 (Clone RM4-4; Biolegend; dilution 1:200). Thymic stromal or thymocyte populations of interest were subsequently sorted using a BD FACS Aria Fusion cell sorter running FACS Diva v8.0.1 (BD Biosciences) using the single-cell sorting mode with a 100 μm nozzle. qRT-PCR was performed as previously described. Briefly, RNA was isolated using the RNAqueous™ Micro Kit for FACS-purified samples (Invitrogen, #AM1931) or the E.Z.N.A.® HP Total RNA Kit (Omega, #R6812) for homogenized whole salivary, liver, lung, pancreas, and white adipose tissues per manufacturer's instructions. cDNA synthesis was performed using a SuperScript

VILO cDNA synthesis kit (Invitrogen) per manufacturer's instructions. cDNA preamplification was performed using the TaqMan PreAmp Master Mix Kit (catalog no. 4384267, ThermoFisher Scientific) per manufacturer's instructions. Quantitative PCR (cycle 1: 95°C for 10 min; cycle 2, x40: 95°C for 15 s and 60°C for 1 min) was performed using a BioRad CFX96 Real-Time System/C1000 Touch Thermal Cycler using presynthesized FAM-MGB TaqMan Gene Expression Assay Probes (ThermoFisher Scientific) to amplify the following genes: *Lpo* (Assay identification [ID]: Mm00475466_m1), *Fgf21* (Assay ID: Mm07297622_g1), *mCherry* (Assay ID: Mr07319438_mr), *Klb* (Assay ID: Mm00473122_m1), *Fgfr1* (Assay ID: Mm00438930_m1), *Fgfr3* (Assay ID: Mm00433294_m1), and pan_Influenza A (Assay ID: Vi99990011_po). qPCR results were analyzed using Bio-Rad CFX Manager software (v3.1.1517.0823). Cq values were normalized to *Hprt* ($2^{-\Delta Cq}$).

Serum/whole thymic tissue analysis of FGF21

Analysis of circulating FGF21 from the serum and whole thymus tissue was performed using the Mouse/Rat FGF-21 Quantikine ELISA Kit (catalog no. MF2100, R&D Systems) according to the manufacturer's recommendations. Briefly, whole blood was collected by cardiac puncture at the time of euthanasia and allowed to clot at room temperature for 30 minutes. Blood samples were spun at 1,000 x g for 10 minutes, then serum was aliquoted and stored at -80°C. Whole protein extracts were obtained from homogenized whole pieces of thymic tissue (5 mg) using the EZLys Tissue Protein Extraction reagent (Abcam, catalog no. ab286872). Samples were kept on ice during homogenization and incubated with protease inhibitors (Thermo Scientific, catalog no. 78429) and DNAse to prevent tissue degradation. After homogenization, samples were pelleted by centrifugation (1,000 x g, 10 mins, 4°C) to remove debris. Supernatant was aliquoted and stored at -80°C. Samples were diluted according to the manufacturer's instructions prior to beginning the ELISA. An Agilent Bio-Tek Synergy LX plate reader was used to obtain the optical density (O.D.) set to 450 nm. Wavelength correction was applied by subtracting readings at 540 nm. A standard curve was created using provided standards and subsequently used to determine the relative concentration of FGF21 (pg/mL) in each sample.

Confocal/Immunofluorescence Imaging

To obtain LPO costaining images in C57BL/6 mice, fresh frozen thymic sections from 3-12-month-old mice were fixed in acetone followed by co-staining with anti-LPO (Proteintech #10376-1-AP; dilution 1:75)/Goat anti-Rabbit Cy5 (Thermo #A10523; dilution 1:100) and anti-EpCAM A488 (Clone G8.8; Biolegend; dilution 1:200). To detect mCherry colocalization in LPO^{FGF21} mice, thymi from 1-month-old mice were fixed overnight in 2% paraformaldehyde while rocking at 4°C, followed by a 10-20% sucrose gradient overnight. 10 µm sections were cut on a cryostat and blocked with 5% FBS in PBS prior to costaining with anti-Ly51 A647 (Clone 6C3; Biolegend; dilution 1:150), anti-DEC 205 A647 (Clone NLDC-45; Biolegend; dilution 1:200), anti-cytokeratin 8 A488 (Clone EP1628Y; Abcam; dilution 1:500); anti-cytokeratin 5 A647 (Clone EP1601Y; Abcam; dilution 1:200), anti-Aire A647 (Clone MM-525; BD Biosciences; dilution 1:150), and UEA1 FITC (Thermo #L32476; dilution 1:200). Sections were stained for 1 hr at room temperature, then washed and coverslipped with Prolong Diamond Antifade Mountant (Thermo #P36961). All images were captured using a Zeiss LSM710 confocal microscope installed with ZEN 2011 software. Endogenous mCherry signal was captured using a 561 nm HeNe1 laser. DAPI was excited using the 405 nm diode laser, A488 signal was detected using a 488 nm argon laser, and A647 signal was captured using a 633 nm HeNe2 laser. Images were captured at 10X and 20X. Identical laser settings were used to capture images from LPO^{WT} and LPO^{FGF21} tissues. Images were subsequently processed using ImageJ software (NIH).

Confetti cTEC image analysis

Thymic sections from LPO^{WT} and LPO^{FGF21} mice crossed with $FoxN1^{Cre}$ $R26^{Confetti}$ reporter mice were imaged using a three-stage sequential scan, as previously described[45]. This method allows for maximum detection of three Confetti fluorescent proteins (cytoplasmic YFP and RFP, and membrane CFP) and simultaneous capture of age-associated autofluorescent pigments that can be removed from reporter images. Briefly, the first scan used 405 nm and 458 nm lasers to excite both CFP and autofluorescent pigments, with collection windows of 463-509 nm (for CFP) and 566-628 nm (for

autofluorescent pigments). The second scan used a 514 nm laser to excite YFP with a collection window of 519-556 nm, and the third scan used a 561 nm laser to excite RFP with a collection window of 566-628 nm. 20x Z-Stacks were acquired on a Zeiss LSM710 confocal microscope. For full color displays, CFP is presented as blue, YFP as yellow, and RFP as red. For qualitative analysis of cTEC morphology, 3D maximum projections were created in ImageJ with a 0.2 pixel minimum filter using the "3D Project" tool. Following acquisition, cTEC area quantification in this study was performed blinded using ImageJ software. Z-Stack images were processed prior to cTEC area quantification using the Stacks -> Z Project -> Average Intensity function. Z-Stack images were then separated into the 3 acquired reporter channels (RFP, YFP, CFP) and the channel capturing autofluorescent pigments, which was removed from the composite image. Channel signal brightness/contrast were optimized for each image using the Image -> Adjust -> Color balance tool. After signals among the 3 channels were equalized within the image, individual cells (defined by any single color surrounded by cells of other colors) contained wholly within the image volume were identified for quantification. cTEC cell area from freehand selections was measured via the Analyze -> Measure tool. The criteria for selection excluded cell areas <400 μm^2 or >3000 μm^2. At least 10-20 cTECs were measured per Z-Stack for a total of 20-40 cTECs quantified per individual mouse. Final quantitation represents 1-2 distinct Z-Stacks from at least 3 independent sex-matched thymuses per group at each age.

Rapamycin-mediated mTOR inhibition

At the time of weaning, 3-week-old LPO^{WT} and LPO^{FGF21} KI mice were injected with 4 mg/kg rapamycin (Thermo Scientific # J62473.EX3) or vehicle via intraperitoneal injection every other day for 2 weeks as previously described[50,53]. At the time of euthanasia, the thymus was harvested, and mTORC1/mTORC2 activation was measured in cTECs, mTECs, and lymphocytes via intracellular flow cytometry as described above. Mouse thymus/body weights and total thymus cellularity via hemocytometer were also determined. Thymocyte CD4/CD8 subsets were also separately stained as described above.

Influenza infection

12-month-old LPO^{WT} and LPO^{FGF21} KI mice were transferred to a BSL-2 facility and allowed to habituate overnight prior to infection. The following day mice were anesthetized with light isoflurane anesthesia and 1000 PFU of mouse-adapted H3N2 influenza (strain A/X-31 H3N2) or H1N1 (strain A/PR8) suspended in 50 µL PBS was intranasally administered to the left nare. Mouse body weights were recorded daily until 10 days post-infection.

Bronchoalveolar lavage (BAL) and analysis of influenza-specific T cells

Upon euthanasia of influenza-infected and/or naïve control mice, the trachea was exposed and a 2-inch-long (75% polyester, 25% cotton) thread was passed underneath the trachea using curved tweezers. An 18-gauge Insyte™ Autoguard™ shielded I.V. catheter (BD) was inserted into the upper trachea and secured using the thread. Brochoalveolar lavage (BAL) was removed by injecting and aspirating 1.0 mL of PBS using a 1 mL PP/PE syringe (Sigma-Aldrich). BAL was placed in a separate tube on ice and the injection and aspiration procedure was repeated another time. Cells were centrifuged (440 x g, 5 mins, 4°C), and cells were resuspended in ice-cold FACS buffer (HBSS, 5% FBS, 0.5% DNAse (1 mg/mL), pH 7.2). Dasatinib (Tocris Bioscience) was added to the cells at a concentration of 50 nM and cells were incubated 30 minutes at 37°C. After incubation, cells were cooled on ice for 5 minutes. Fc receptors were blocked with CD16/CD32 (eBioscience; #:14-0161-81; dilution 1:130) for 10 minutes on ice. Cells were then stained with 0.5 µg of $NP_{366-374}/D^b$ (NP) tetramers and incubated protected from light for 1 hour at 25°C. Cells were then washed with sorting buffer and then stained with a cocktail containing fluorescent antibodies conjugated against CD8-V500 (Clone 53-6.7; BD Biosciences; dilution 1:100), CD4-FITC (Clone RM4-4; Invitrogen; dilution 1:200), CD90.2-PerCPeFluor710 (Clone 30-H12; Invitrogen; dilution 1:200), and CD44-BV510 (Clone IM7; Biolegend; dilution 1:200) on ice for 30 minutes. Cells were washed and suspended in sorting buffer for FACS analysis. NP-tetramer$^+$ cells were analyzed on $CD90.2^+CD8^+$ singlet lymphocytes using a Cytek

Aurora flow cytometer running SpectroFlo v3.3.0 and FlowJo v10.9 flow cytometry analysis software (Tree Star).

Antinuclear antibody evaluation

The presence of ANAs was evaluated in serum of 10-12-month-old LPO^{WT} and LPO^{FGF21} mice. 25 µL serum (1:100 dilution) was added to HEp-2 slides (MBL International, AN-1012) and incubated at room temperature for 30 minutes. Slides were washed twice and then sample wells were incubated with FITC-conjugated anti-IgG (poly4060, Biolegend; dilution 1:100) for 30 minutes. Slides were washed and coverslipped with Vectashield Vibrance with DAPI (Vector Laboratories). Images were captured at 10X and 20X magnification using a Zeiss LSM710 microscope. Samples were coded and evaluation was performed blinded. Laser settings for the FITC channel were kept identical between each sample.

Tissue lymphocytic infiltration studies

Lung, liver, and salivary gland tissue harvested from 10-12-month-old LPO^{WT} and LPO^{FGF21} mice were fixed for 24 hours in 10% NBF and blocked in paraffin. Slides were cut and stained with H&E. Sections from at least three different anatomic areas were examined for lymphocytic infiltration in each tissue. Samples were coded and evaluated for the presence of lymphocytic infiltrates blinded.

Statistics and Reproducibility

All data were analyzed using Excel (Microsoft) and GraphPad Prism 10 software (La Jolla, California). Statistical significance ($p < 0.05$) was computed using two-tailed unpaired Student's t-test, ordinary one way-ANOVA (analysis of variance), or two way-ANOVA, as indicated in the figure legends. Tukey's multiple comparisons test was performed following significant one way- and two way-ANOVA tests. No statistical method was used to predetermine sample size, but our sample sizes are similar to those reported in previous publications[32, 87]. Sample sizes for each experiment are indicated in the figure legends. At least three biological replicates per group were used for all experiments. No animals

or data were excluded from our analyses. No randomization method was used. Except where noted (evaluation of ANA positivity, glymphocytic infiltrates, and cTEC size analysis), investigators were not blinded to group allocation during analysis. Data distribution was assumed to be normal, but this was not formally tested.

Data Availability

All data and methods supporting the findings found in the article can be obtained from the corresponding author upon reasonable request. Source data are provided with this paper. Single-cell transcriptomic data used to quantify *Fgf21* and *Lpo* expression among TEC populations can be accessed via ArrayExpress with accession number E-MTAB-8560[25]. Global transcriptional profiles from microdissected whole cortical and medullary tissue can be accessed via the Gene Expression Omnibus public database (www.ncbi.nlm.nih.gov/geo/query/acc.cgi?acc) with accession number GSE:132136[45]. Microarray datasets used to determine regulation of thymic *Lpo* expression by Aire and Fezf2 can be accessed via the Gene Expression Omnibus public database with accession numbers GSE:14365[58] (Aire) and GSE:69105[59] (Fezf2).

Acknowledgments

We sincerely thank Raehum Paik and Selika Garza at UT Health San Antonio for their efforts to create the LPO^{FGF21} line. We also thank Howard Petrie (Herbert Wertheim UF Scripps Institute for Biomedical Innovation & Technology) for technical advice. We thank Drs. Adam B. Salmon and James F. Nelson for helpful discussions and comments on the manuscript. Confocal images were generated in the Core Optical Imaging Facility, which is supported by UT Health San Antonio and NIH-NCI P30 CA54174. Flow cytometry samples were analyzed via The Flow Cytometry Shared Resource at UT Health San Antonio, which is supported by a grant from the National Cancer Institute (P30CA054174) to the Mays Cancer Center, a grant from the Cancer Prevention and Research Institute of Texas (CPRIT) (RP210126), a grant from the National Institutes of Health (S10OD030432), and support from the Office of the Vice President for Research at UT Health San Antonio. Formalin-fixed tissues were prepared for H&E staining at the STRL UTHSCSA Histology/Immunohistochemistry Laboratory. This

work was supported by NIH Public Health Service grants R01AG086271, R21AI154109, and R21AG081709 (A.V.G.), funds from UT Health San Antonio (A.V.G.), and by NIH Graduate Research in Immunology Program (GRIP) fellowship T32 AI138944 (S.A.W.). This work was also supported in part by the generosity of an anonymous donor to Stanford University establishing the DiGeorge Syndrome Research Fund (G.A.H.), Swiss National Science Foundation grant IZLJZ3_171050; 310030_184672 (G.A.H.), Medical Research Council grant MR/S036407/1 (G.A.H.), Wellcome Trust grant 105045/Z/14/Z and 211944/Z/18/Z (G.A.H).

Author Contributions

S.A.W., G.A.H., and A.V.G. designed research; S.A.W., N.E.J., I.G.A.R., F.M.G., Y.X., T.V., M.K.S., A.K.G., K.S.A., K.L.W., and A.V.G. performed research; S.A.W., N.E.J., I.G.A.R., F.M.G., T.V., and A.V.G. analyzed data; and S.A.W. and A.V.G. wrote the manuscript.

Conflict of Interest

The authors declare no competing interests.

Figure Legends

Fig. 1: Characterization of *Fgf21* expression in TECs and identification of Lpo (Lactoperoxidase) as an appropriate candidate for driving broad, constitutive *Fgf21* expression in medullary thymic epithelial cells throughout the lifespan.

a, *Fgf21* relative expression levels and frequencies among 9 distinct TEC populations (proliferating TEC (MHC-II^{+}, Ly6d^{-}), tuft-like mTEC (*Avil*^{hi}*, Trpm5*^{hi}*)*, post-Aire mTEC (*Krt80*^{hi}*, Spink5*^{hi}*)*, mature mTEC (*Aire*^{hi}, *Cd52*^{hi}*)*, intertypical TEC (*Ccl21a*^{hi}*, Krt5*^{hi}*)*, perinatal cTEC (*Syngr1*^{hi}, *Gper1*^{hi}*)*, mature cTEC (*Prss16*^{hi}*, Cxcl12*^{hi}*)*, neural TEC/nTEC (*Sod3*^{hi}, *Dpt*^{hi}*)*, structural TEC/sTEC (*Cd177*^{hi}*, Car8*^{hi}) were obtained from the thymi of mice aged 1, 4, 16, 32, and 52 weeks using a previously published scRNA-seq dataset[25]. **b,** Changes in relative abundance of TEC populations described in **(a)** present in the murine thymus from the early postnatal period (1-4 weeks) to one year of age. **c,** Schematic diagram outlining the selection criteria for prioritizing candidate pan-mTEC genes. Top candidates

were selected using a published transcriptional database consisting of global transcriptional profiles generated from cortical and medullary lymphocytes, microdissected whole cortical and medullary tissue (GEO: GSE132136)[45]. Aire-dependent genes were excluded based on prior published Aire-regulated gene lists[56, 57]. The candidate genes were ranked using gene expression levels (Gcrma values) and intensity skew (based on BioGPS expression values), followed by immunofluorescence microscopy validation to identify expression patterns in thymus. **d,** Frozen 5 micron sections from 3-month- and 12-month-old C57BL/6 mouse thymi (n=3 per group) were co-stained with DAPI, anti-LPO/Goat anti-Rabbit Cy5 (red), and anti-EpCAM (CD326) A488 (green). Representative images are shown at 20x magnification. Scale bar= 50 μm. **e,** Schematic diagram of the Lpo-Fgf21-mCherry knock-in allele. A bicistronic vector was designed allowing for the insertion of *Fgf21* and mCherry cDNA at the end of Exon 13 of the *Lpo* gene through incorporation of P2A and T2A peptide sequences.

Fig. 2: Flow cytometric evaluation of mCherry expression in the LPO^{FGF21} knock-in (KI) thymus confirms broad and specific expression of the KI allele in mTEC subsets.

a, Flow cytometry gating strategy (pre-gated on viable singlets) used for the identification of cTEC (CD45.2$^-$, EpCAM$^+$, Ly51$^+$, UEA1$^-$), total mTEC (CD45.2$^-$, EpCAM$^+$, Ly51$^-$, UEA1$^+$), mTEC^{lo} (CD45.2$^-$, EpCAM$^+$, Ly51$^-$, MHCII^{lo}, CD80^{lo}), mTEC^{hi} (CD45.2$^-$, EpCAM$^+$, Ly51$^-$, MHCII^{hi}, CD80^{hi}), cDC (CD45.2$^+$, CD11c$^+$, B220$^-$), pDC (CD45.2$^+$, CD11c$^+$, B220$^+$), endothelial cell (EC) (CD45.2$^-$, EpCAM$^-$, CD31$^+$), pericyte (PC) (CD45.2$^-$, EpCAM$^-$, CD31$^-$, PDGFRαβ$^+$, CD146$^+$, gp38$^-$), and fibroblast (Fb) (CD45.2$^-$, EpCAM$^-$, CD31$^-$, PDGFRαβ$^+$, CD146$^-$, gp38$^+$) subsets from thymi of the indicated mice after enzymatic digestion and stromal cell enrichment. **b,** Representative histograms of mCherry expression among mTEC, DC, endothelial, and mesenchymal subsets of 1-month-old LPO^{WT} (n=4) and LPO^{FGF21} mice (n=5). **c,** The frequency of mCherry$^+$ cells among cTEC, mTEC, DC, endothelial, and mesenchymal subsets was quantified in LPO^{FGF21} KI mice (n=5). Data among mTEC subsets were analyzed by one-way ANOVA followed by Tukey's multiple comparisons test. Horizontal lines indicate significant comparisons among mTEC subsets. ns= p≥0.05. Mean and SEM indicated by horizontal lines. Each symbol represents an individual mouse. Data are representative of three independent experiments.

d, Representative confocal microscopy images of thymic mCherry expression (red) at 10x (left) and 20x (right, magnified view of the indicated 10x region) magnification from LPO^{FGF21} (n=5) 1-month-old mice. Thymic sections were stained with anti-cytokeratin 5 A647. Scale bar= 100 μm (10x), 50 μm (20x).

Fig. 3: Overexpression of FGF21 in LPO^{FGF21} KI mTECs results in increased thymus size and diminishes age-associated thymic atrophy.

a, Thymus weight/body weight ratios (somatic index) of LPO^{WT} and LPO^{FGF21} KI female mice at 1 month (n=7 per group), 3 months (n=5 per group), and 12 months of age (n=6 per group). **b,** Total thymus cellularity was determined in LPO^{WT} and LPO^{FGF21} KI female mice at 1 month (n=8 LPO^{WT}, n=7 LPO^{FGF21}), 3 months (n=9 LPO^{WT}, n=8 LPO^{FGF21}), and 12 months of age (n=9 LPO^{WT}, n=7 LPO^{FGF21}). **c,d,** Thymocyte $CD4^-CD8^-$ DN, $CD4^+CD8^+$ DP, $CD4^+$ SP, and $CD8^+$ SP subset frequency (**c**) and total cell number (**d**), as well as the frequency and total number of cTEC ($CD45.2^-$, $EpCAM^+$, $Ly51^+$) and mTEC ($CD45.2^-$, $EpCAM^+$, $Ly51^-$), were quantified in 1-month-old (n=6 LPO^{WT}, n=10 LPO^{FGF21}) (top) and 13-month-old (bottom) (n=5 LPO^{WT}, n=6 LPO^{FGF21}) LPO^{WT} and LPO^{FGF21} KI female mice. Data were analyzed via two-sided Student's t-tests (**a-d**). ns= p≥0.05, *= p<0.05, **= p<0.005, ***= p<0.001, ****= p<0.0001. Mean and SEM are indicated by horizontal lines. Each symbol represents an individual mouse. Data are representative of three or more experiments.

Fig. 4: mTORC1 and mTORC2 activity in cortical thymic epithelial cells are distinctly and dynamically regulated by paracrine FGF21 signaling during thymus growth and atrophy.

a,b, Representative histograms (top) and MFI (bottom) of $p4EBP1^{T36,T45}$ (**a**) and $pAkt^{S473}$ (**b**) in cTECs ($CD45.2^-$, $EpCAM^+$, $Ly51^+$), mTECs ($CD45.2^-$, $EpCAM^+$, $Ly51^-$), and $CD45.2^+$ lymphocytes from thymi of 3-week-old (n=4) and 6-month-old (n=6) C57BL/6 mice. Single cell suspensions of enriched thymic stromal cells were stained with fluorescent antibodies targeting $p4EBP1^{T36,T45}$ and $pAkt^{S473}$ following fixation and permeabilization. **c,d,** Representative histograms (top) and MFI (bottom) demonstrating $p4EBP1^{T36,T45}$ (**c**) and $pAkt^{S473}$ (**d**) activation in cTEC of 2.5-week-old (n=5 LPO^{WT}, n=6 LPO^{FGF21}), 3-month-old (n=4 LPO^{WT}, n=4 LPO^{FGF21}), and 12-month-old (n=4 LPO^{WT}, n=6 LPO^{FGF21}) LPO^{WT} and

LPO^{FGF21} KI female mice. **e,** Representative histograms (left) and MFI (right) of TSC1 expression in cTECs from LPO^{WT} mice at 2.5 weeks, 6 weeks, and 4 months of age (n=4 per group). Data were analyzed via two-sided student's t-test (**a-d**) or one-way ANOVA with Tukey's multiple comparisons test (**e**). ns= p≥0.05, *= p<0.05, **= p<0.01, ***= p<0.001, ****= p<0.0001. Mean and SEM indicated by horizontal lines. Each symbol represents an individual mouse. Data are representative of three or more experiments. **f,** Expression of manually curated mTORC1-(red/green) and mTORC2-(blue) regulated genes throughout course of post-castration regeneration is normalized to 12-month-old untreated thymus, which also represents day 0 of the regeneration sequence.

Fig. 5: Pharmacological mTOR inhibition mitigates the impact of FGF21 overexpression on DP thymocyte number and mTORC1 signaling in cTECs.

a, Schematic of experimental approach. LPO^{WT} and LPO^{FGF21} KI mice were treated with 4 mg/kg rapamycin or vehicle via intraperitoneal injection every other day for two weeks, beginning at the time of weaning (3 weeks of age). At the time of euthanasia, the thymus was harvested, and subsequently thymus weight/body weight ratios, total thymus cellularity, thymocyte subset frequencies, and mTORC1/mTORC2 activation in cTECs, mTECs, and lymphocytes were determined. **b,** Thymus weight/body weight ratio was determined in LPO^{WT} vehicle-treated (n=4), LPO^{WT} rapamycin-treated (n=4), LPO^{FGF21} KI vehicle-treated (n=4), and LPO^{FGF21} KI rapamycin-treated (n=4) mice. **c,** Total thymus cellularity was estimated in LPO^{WT} vehicle-treated (n=4), LPO^{WT} rapamycin-treated (n=4), LPO^{FGF21} KI vehicle-treated (n=4), and LPO^{FGF21} KI rapamycin-treated (n=4) mice. **d,** Thymocyte CD4^{-} CD8^{-} DN, CD4^{+}CD8^{+} DP, CD4^{+} SP, and CD8^{+} SP subset frequency (top) and total cell number (bottom) were estimated in LPO^{WT} vehicle-treated (n=4), LPO^{WT} rapamycin-treated (n=4), LPO^{FGF21} KI vehicle-treated (n=4), and LPO^{FGF21} KI rapamycin-treated (n=4) mice. **e,f,** MFI of pS6$^{S235-236}$ (**e**) and pAkt^{S473} (**f**) in cTEC, mTEC, and CD45.2^{+} lymphocytes were measured in LPO^{WT} vehicle-treated (n=4), LPO^{WT} rapamycin-treated (n=4), LPO^{FGF21} KI vehicle-treated (n=4), and LPO^{FGF21} KI rapamycin-treated (n=4) mice. Data were analyzed via two-way ANOVA followed by Tukey's multiple comparisons test (**b-f**). ns= p≥0.05, *= p<0.05, **= p<0.01, ***= p<0.001, ****= p<0.0001. Mean and

SEM are indicated by horizontal lines. Each symbol represents an individual mouse. Data are the result of two independent experiments. Schematic in (**a**) created in https://BioRender.com.

Fig. 6: FGF21 overexpression in mTECs mitigates waning naïve T cell frequency and T cell responsiveness to influenza infection in older mice.

a,b, Representative gating strategy showing isolation of $CD62L^+$, $CD44^{lo}$ naïve T cells and $CD62L^+$, $CD44^{hi}$ memory T cells from (**a**) $CD3^+$, $CD8^+$ and (**b**) $CD3^+$, $CD4^+$ splenocytes in 2-month-old and 12-month-old LPO^{WT} and LPO^{FGF21} mice. **c,d,** $CD8^+$ (**c**) and $CD4^+$ (**d**) naïve:memory ratios were quantified in splenocytes of 2-month-old and 12-month-old LPO^{WT} and LPO^{FGF21} mice (n=6 per group). Data were analyzed via Student's t-tests. ns= $p \geq 0.05$, **= $p < 0.01$. **e,** Schematic diagram demonstrating influenza infection timeline. 12-month-old LPO^{WT} (n=6) and LPO^{FGF21} (n=6) mice were infected with 1000 PFU influenza A X31 virus via intranasal challenge. Body weights were recorded from 0-10 dpi. Upon euthanasia thymus, spleen, mediastinal lymph nodes (MLN), and bronchiolar lavage (BAL) were collected for staining with $NP_{366-374}$-specific tetramers. Spleen and thymus total size were estimated via cell counting. Lung tissue was also collected for influenza mRNA quantification. **f,** Overall % body weight lost throughout the course of infection was determined by comparing body weight at 0-10 dpi from baseline body weight in influenza-infected LPO^{WT} and LPO^{FGF21} mice (n=6 per group, 3 independent experiments). **g,** Thymus size was determined 10 dpi in LPO^{WT} and LPO^{FGF21} mice (n=6 per group) via counting with hemocytometer. **h,** Influenza viral mRNA was quantified in lung tissue harvested 10 dpi in LPO^{WT} and LPO^{FGF21} mice (n=6 per group). **i,j,** The relative frequency (**i**) and total number (**j**) of $NP_{366-374}$-specific $CD90.2^+$, $CD8^+$ T cells in BAL, MLN, and spleen in influenza-infected LPO^{WT} and LPO^{FGF21} mice (n=6 per group) were quantified 10 dpi via flow cytometry. Data were analyzed via two-sided Student's t-tests (**c-j**). ns= $p \geq 0.05$, *= $p < 0.05$, **= $p < 0.01$, ***=$p < 0.001$, ****= $p < 0.0001$. Mean and SEM are indicated by horizontal lines. Each symbol represents an individual mouse. Data are the result of two independent experiments. Schematic in (**a**) created in https://BioRender.com.

Fig. 7: Persistent medullary TEC-driven overexpression of FGF21 protects against age-associated impairments in clonal deletion and development of peripheral autoimmunity.

a, Gating strategy used to detect clonal deletion among early ($CCR7^-$) and late ($CCR7^+$) $lineage^-$ ($CD19^-$, $CD25^-$, $TCR\gamma\delta^-$, $NK1.1^-$) signaled ($CD5^+$, $TCR\beta^+$) T cells. **b,c,** The frequency of cleaved caspase 3^+ cells was quantified among early and late signaled T cells in 2-month-old LPO^{WT} and $LPO^{FGF21/FGF21}$ homozygous mice (n=5 per group) and in 12-month-old LPO^{WT} and $LPO^{FGF21/FGF21}$ homozygous mice (n=5 per group). Data were analyzed by two-way ANOVA followed by Tukey's multiple comparisons test. Mean and SEM are indicated by horizontal lines. Significant comparisons are indicated (*= p<0.05, **= p<0.01, ***= p<0.001, ****= p<0.0001) **d,** The presence of antinuclear antibodies was assessed in serum from 12-month-old LPO^{WT} and LPO^{FGF21} mice (n=8 per group). Serum was incubated on HEp-2-coated slides, followed by immunostaining with anti-mouse IgG FITC. The number of animals that tested positive for ANAs are indicated in the IgG channel image. Images are at 20x magnification. Scale bar= 50 μm. **e,** Liver, lung, and salivary tissue were harvested from 12-month-old LPO^{WT} and LPO^{FGF21} (n=7 per group) and evaluated for the presence of lymphocytic infiltrates via H&E staining (indicated via arrows). The number of mice testing positive for infiltrates are indicated in each tissue. Scale bar= 50 μm (20x). **f,** Representative plots showing the gating strategy determining the frequency of $CD4^+$ Tregs ($CD4^+$ $CD8^-$ $CD25^+$ $Foxp3^+$) (top) and $Helios^+/Helios^-$ $CD4^+$ Tregs (bottom) among splenocytes in 2-month-old and 12-month-old LPO^{WT} and LPO^{FGF21} mice (n=3 per group). **g-i,** The frequency of $CD4^+$ Tregs (**g**), $Helios^+$ $CD4^+$ Tregs (**h**), and $Helios^–$ $CD4^+$ Tregs (**i**) were compared between 2-month-old (n=3 per group) and 12-month-old (n=3 per group) LPO^{WT} and LPO^{FGF21} mice by one-way ANOVA followed by Tukey's multiple comparisons test. Mean and SEM are indicated by horizontal lines. Significant comparisons are indicated (*= p<0.05, **= p<0.01, ***= p<0.001, ****= p<0.0001).

Fig. 8. Paracrine thymic FGF21 signaling increases cTEC size during aging.

a-d, Representative maximum intensity Z-Stack 3D projections taken from 60 μm optical stacks (20x magnification) from 1-month-old $FoxN1^{Cre}$ $R26^{Confetti}$ LPO^{WT} (n=4 biological replicates), 1-month-old

FoxN1^{Cre} R26^{Confetti} LPO^{FGF21} (n=4), 6-month-old FoxN1^{Cre} R26^{Confetti} LPO^{WT} (n=3), and 6-month-old FoxN1^{Cre} R26^{Confetti} LPO^{FGF21} (n=5) thymic sections. Scale bar= 50 μm. 3D animations can be found in Supplementary Movies 1-4. **e**, cTEC area (μm^2) was quantified from Z-Stack projections from thymic sections from 1-month-old FoxN1^{Cre} R26^{Confetti} LPO^{WT} (n=4), 1-month-old FoxN1^{Cre} R26^{Confetti} LPO^{FGF21} (n=4), 6-month-old FoxN1^{Cre} R26^{Confetti} LPO^{WT} (n=3), and 6-month-old FoxN1^{Cre} R26^{Confetti} LPO^{FGF21} (n=5) mice via blinded analysis with ImageJ software. Each symbol represents a single cTEC. Red horizontal lines represent mean ± SEM. Data were analyzed by one-way ANOVA with Tukey's multiple comparisons. ns= p≥0.05, ****=p<0.0001.

References

1. Goldschneider, I., Komschlies, K.L. & Greiner, D.L. Studies of thymocytopoiesis in rats and mice. I. Kinetics of appearance of thymocytes using a direct intrathymic adoptive transfer assay for thymocyte precursors. *The Journal of experimental medicine* **163**, 1-17 (1986).

2. Foss, D.L., Donskoy, E. & Goldschneider, I. The importation of hematogenous precursors by the thymus is a gated phenomenon in normal adult mice. *The Journal of experimental medicine* **193**, 365-374 (2001).

3. Petrie, H.T. & Zuniga-Pflucker, J.C. Zoned out: functional mapping of stromal signaling microenvironments in the thymus. *Annual review of immunology* **25**, 649-679 (2007).

4. Klug, D.B. *et al.* Interdependence of cortical thymic epithelial cell differentiation and T-lineage commitment. *Proceedings of the National Academy of Sciences of the United States of America* **95**, 11822-11827 (1998).

5. Klein, L., Kyewski, B., Allen, P.M. & Hogquist, K.A. Positive and negative selection of the T cell repertoire: what thymocytes see (and don't see). *Nature reviews. Immunology* **14**, 377-391 (2014).

6. Abramson, J. & Anderson, G. Thymic Epithelial Cells. *Annual review of immunology* **35**, 85-118 (2017).

7. Qi, Q. *et al.* Diversity and clonal selection in the human T-cell repertoire. *Proceedings of the National Academy of Sciences of the United States of America* **111**, 13139-13144 (2014).

8. Douek, D.C. *et al.* Changes in thymic function with age and during the treatment of HIV infection. *Nature* **396**, 690-695 (1998).

9. Jamieson, B.D. *et al.* Generation of functional thymocytes in the human adult. *Immunity* **10**, 569-575 (1999).

10. Thome, J.J. *et al.* Longterm maintenance of human naive T cells through in situ homeostasis in lymphoid tissue sites. *Sci Immunol* **1** (2016).

11. Bains, I., Thiebaut, R., Yates, A.J. & Callard, R. Quantifying thymic export: combining models of naive T cell proliferation and TCR excision circle dynamics gives an explicit measure of thymic output. *J Immunol* **183**, 4329-4336 (2009).

12. Steinmann, G.G., Klaus, B. & Muller-Hermelink, H.K. The involution of the ageing human thymic epithelium is independent of puberty. A morphometric study. *Scand J Immunol* **22**, 563-575 (1985).

13. Mitchell, W.A., Lang, P.O. & Aspinall, R. Tracing thymic output in older individuals. *Clin Exp Immunol* **161**, 497-503 (2010).

14. Hartwig, M. & Steinmann, G. On a causal mechanism of chronic thymic involution in man. *Mechanisms of ageing and development* **75**, 151-156 (1994).

15. Aspinall, R., Pitts, D., Lapenna, A. & Mitchell, W. Immunity in the elderly: the role of the thymus. *Journal of comparative pathology* **142 Suppl 1**, S111-115 (2010).

16. Haynes, B.F., Sempowski, G.D., Wells, A.F. & Hale, L.P. The human thymus during aging. *Immunologic research* **22**, 253-261 (2000).

17. Hale, J.S., Boursalian, T.E., Turk, G.L. & Fink, P.J. Thymic output in aged mice. *Proceedings of the National Academy of Sciences of the United States of America* **103**, 8447-8452 (2006).

18. Ernst, D.N. *et al.* Differences in the expression profiles of CD45RB, Pgp-1, and 3G11 membrane antigens and in the patterns of lymphokine secretion by splenic CD4+ T cells from young and aged mice. *J Immunol* **145**, 1295-1302 (1990).

19. Utsuyama, M. *et al.* Differential age-change in the numbers of CD4+CD45RA+ and CD4+CD29+ T cell subsets in human peripheral blood. *Mechanisms of ageing and development* **63**, 57-68 (1992).

20. Palmer, S., Albergante, L., Blackburn, C.C. & Newman, T.J. Thymic involution and rising disease incidence with age. *Proceedings of the National Academy of Sciences of the United States of America* **115**, 1883-1888 (2018).

21. Keilich, S.R., Bartley, J.M. & Haynes, L. Diminished immune responses with aging predispose older adults to common and uncommon influenza complications. *Cell Immunol* **345**, 103992 (2019).

22. Brien, J.D., Uhrlaub, J.L., Hirsch, A., Wiley, C.A. & Nikolich-Zugich, J. Key role of T cell defects in age-related vulnerability to West Nile virus. *The Journal of experimental medicine* **206**, 2735-2745 (2009).

23. Nikolich-Zugich, J. & Rudd, B.D. Immune memory and aging: an infinite or finite resource? *Current opinion in immunology* **22**, 535-540 (2010).

24. Haynes, L., Eaton, S.M., Burns, E.M., Randall, T.D. & Swain, S.L. CD4 T cell memory derived from young naive cells functions well into old age, but memory generated from aged naive cells functions poorly. *Proceedings of the National Academy of Sciences of the United States of America* **100**, 15053-15058 (2003).

25. Baran-Gale, J. *et al.* Ageing compromises mouse thymus function and remodels epithelial cell differentiation. *Elife* **9** (2020).

26. Bredenkamp, N., Nowell, C.S. & Blackburn, C.C. Regeneration of the aged thymus by a single transcription factor. *Development* **141**, 1627-1637 (2014).

27. Coder, B.D., Wang, H., Ruan, L. & Su, D.M. Thymic involution perturbs negative selection leading to autoreactive T cells that induce chronic inflammation. *J Immunol* **194**, 5825-5837 (2015).

28. Muller, L. & Pawelec, G. As we age: Does slippage of quality control in the immune system lead to collateral damage? *Ageing research reviews* **23**, 116-123 (2015).

29. Thomas, R., Wang, W. & Su, D.M. Contributions of Age-Related Thymic Involution to Immunosenescence and Inflammaging. *Immun Ageing* **17**, 2 (2020).

30. Xia, J. *et al.* Age-Related Disruption of Steady-State Thymic Medulla Provokes Autoimmune Phenotype via Perturbing Negative Selection. *Aging Dis* **3**, 248-259 (2012).

31. Lancaster, J.N. *et al.* Central tolerance is impaired in the middle-aged thymic environment. *Aging Cell* **21**, e13624 (2022).

32. Hester, A.K. *et al.* Redox regulation of age-associated defects in generation and maintenance of T cell self-tolerance and immunity to foreign antigens. *Cell Rep* **38**, 110363 (2022).

33. Kooshesh, K.A., Foy, B.H., Sykes, D.B., Gustafsson, K. & Scadden, D.T. Health Consequences of Thymus Removal in Adults. *N Engl J Med* **389**, 406-417 (2023).

34. Sutherland, J.S. *et al.* Activation of thymic regeneration in mice and humans following androgen blockade. *J Immunol* **175**, 2741-2753 (2005).

35. Rode, I. & Boehm, T. Regenerative capacity of adult cortical thymic epithelial cells. *Proceedings of the National Academy of Sciences of the United States of America* **109**, 3463-3468 (2012).

36. Heng, T.S. *et al.* Impact of sex steroid ablation on viral, tumour and vaccine responses in aged mice. *PLoS One* **7**, e42677 (2012).

37. Cepeda, S. & Griffith, A.V. Thymic stromal cells: Roles in atrophy and age-associated dysfunction of the thymus. *Exp Gerontol* **105**, 113-117 (2018).

38. Fahy, G.M. *et al.* Reversal of epigenetic aging and immunosenescent trends in humans. *Aging Cell* **18**, e13028 (2019).

39. Rossi, S.W. *et al.* Keratinocyte growth factor (KGF) enhances postnatal T-cell development via enhancements in proliferation and function of thymic epithelial cells. *Blood* **109**, 3803-3811 (2007).

40. Hakim, F.T. *et al.* Age-dependent incidence, time course, and consequences of thymic renewal in adults. *The Journal of clinical investigation* **115**, 930-939 (2005).

41. Masters, A.R., Haynes, L., Su, D.M. & Palmer, D.B. Immune senescence: significance of the stromal microenvironment. *Clin Exp Immunol* **187**, 6-15 (2017).

42. Griffith, A.V., Fallahi, M., Venables, T. & Petrie, H.T. Persistent degenerative changes in thymic organ function revealed by an inducible model of organ regrowth. *Aging Cell* **11**, 169-177 (2012).

43. Gray, D.H. *et al.* Unbiased analysis, enrichment and purification of thymic stromal cells. *Journal of immunological methods* **329**, 56-66 (2008).

44. Mohtashami, M. & Zuniga-Pflucker, J.C. Three-dimensional architecture of the thymus is required to maintain delta-like expression necessary for inducing T cell development. *J Immunol* **176**, 730-734 (2006).

45. Venables, T., Griffith, A.V., DeAraujo, A. & Petrie, H.T. Dynamic changes in epithelial cell morphology control thymic organ size during atrophy and regeneration. *Nat Commun* **10**, 4402 (2019).

46. Griffith, A.V. *et al.* Spatial mapping of thymic stromal microenvironments reveals unique features influencing T lymphoid differentiation. *Immunity* **31**, 999-1009 (2009).

47. Dumas, S.N. & Lamming, D.W. Next Generation Strategies for Geroprotection via mTORC1 Inhibition. *J Gerontol A Biol Sci Med Sci* **75**, 14-23 (2020).

48. Goldberg, E.L. *et al.* Lifespan-extending caloric restriction or mTOR inhibition impair adaptive immunity of old mice by distinct mechanisms. *Aging Cell* **14**, 130-138 (2015).

49. Youm, Y.H., Horvath, T.L., Mangelsdorf, D.J., Kliewer, S.A. & Dixit, V.D. Prolongevity hormone FGF21 protects against immune senescence by delaying age-related thymic involution. *Proceedings of the National Academy of Sciences of the United States of America* **113**, 1026-1031 (2016).

50. Nakayama, Y. *et al.* Fgf21 regulates T-cell development in the neonatal and juvenile thymus. *Sci Rep* **7**, 330 (2017).

51. Ding, X. *et al.* betaKlotho is required for fibroblast growth factor 21 effects on growth and metabolism. *Cell Metab* **16**, 387-393 (2012).

52. Ogawa, Y. *et al.* BetaKlotho is required for metabolic activity of fibroblast growth factor 21. *Proceedings of the National Academy of Sciences of the United States of America* **104**, 7432-7437 (2007).

53. Bornstein, C. *et al.* Single-cell mapping of the thymic stroma identifies IL-25-producing tuft epithelial cells. *Nature* **559**, 622-626 (2018).

54. Klein, F. *et al.* Combined multidimensional single-cell protein and RNA profiling dissects the cellular and functional heterogeneity of thymic epithelial cells. *Nat Commun* **14**, 4071 (2023).

55. Nitta, T. *et al.* Fibroblasts as a source of self-antigens for central immune tolerance. *Nature immunology* **21**, 1172-1180 (2020).

56. Johnnidis, J.B. *et al.* Chromosomal clustering of genes controlled by the aire transcription factor. *Proceedings of the National Academy of Sciences of the United States of America* **102**, 7233-7238 (2005).

57. Derbinski, J. *et al.* Promiscuous gene expression in thymic epithelial cells is regulated at multiple levels. *The Journal of experimental medicine* **202**, 33-45 (2005).

58. Hubert, F.X. *et al.* Aire-deficient C57BL/6 mice mimicking the common human 13-base pair deletion mutation present with only a mild autoimmune phenotype. *J Immunol* **182**, 3902-3918 (2009).

59. Takaba, H. *et al.* Fezf2 Orchestrates a Thymic Program of Self-Antigen Expression for Immune Tolerance. *Cell* **163**, 975-987 (2015).

60. Ki, S. *et al.* Global transcriptional profiling reveals distinct functions of thymic stromal subsets and age-related changes during thymic involution. *Cell Rep* **9**, 402-415 (2014).

61. Youm, Y., Gliniak, C., Zhang, Y., Dlugos, T., Scherer, P., Deep Dixit, V. Enhanced paracrine action of FGF21 in stromal cells delays thymic aging. *Nat Aging* (2024).

62. Villarroya, J. *et al.* Aging is associated with increased FGF21 levels but unaltered FGF21 responsiveness in adipose tissue. *Aging Cell* **17**, e12822 (2018).

63. Minard, A.Y. *et al.* mTORC1 Is a Major Regulatory Node in the FGF21 Signaling Network in Adipocytes. *Cell Rep* **17**, 29-36 (2016).

64. Guertin, D.A. *et al.* Ablation in mice of the mTORC components raptor, rictor, or mLST8 reveals that mTORC2 is required for signaling to Akt-FOXO and PKCalpha, but not S6K1. *Dev Cell* **11**, 859-871 (2006).

65. Liang, Z. *et al.* MTOR signaling is essential for the development of thymic epithelial cells and the induction of central immune tolerance. *Autophagy* **14**, 505-517 (2018).

66. Semwal, M.K., Jones, N.E. & Griffith, A.V. Metabolic Regulation of Thymic Epithelial Cell Function. *Front Immunol* **12**, 636072 (2021).

67. Wang, H.X., Cheng, J.S., Chu, S., Qiu, Y.R. & Zhong, X.P. mTORC2 in Thymic Epithelial Cells Controls Thymopoiesis and T Cell Development. *J Immunol* **197**, 141-150 (2016).

68. Wang, H.X. *et al.* mTORC1 in Thymic Epithelial Cells Is Critical for Thymopoiesis, T-Cell Generation, and Temporal Control of gammadeltaT17 Development and TCRgamma/delta Recombination. *PLoS Biol* **14**, e1002370 (2016).

69. Laplante, M. & Sabatini, D.M. Regulation of mTORC1 and its impact on gene expression at a glance. *J Cell Sci* **126**, 1713-1719 (2013).

70. Liu, G.Y. & Sabatini, D.M. mTOR at the nexus of nutrition, growth, ageing and disease. *Nat Rev Mol Cell Biol* **21**, 183-203 (2020).

71. Maiti, S., Mondal, S., Satyavarapu, E.M. & Mandal, C. mTORC2 regulates hedgehog pathway activity by promoting stability to Gli2 protein and its nuclear translocation. *Cell Death Dis* **8**, e2926 (2017).

72. Chen, C. *et al.* TSC-mTOR maintains quiescence and function of hematopoietic stem cells by repressing mitochondrial biogenesis and reactive oxygen species. *The Journal of experimental medicine* **205**, 2397-2408 (2008).

73. Chen, C., Liu, Y., Liu, Y. & Zheng, P. mTOR regulation and therapeutic rejuvenation of aging hematopoietic stem cells. *Sci Signal* **2**, ra75 (2009).

74. Overall, S.A., van Driel, I.R. & Gleeson, P.A. Rapamycin results in Bim-mediated loss of thymic regulatory T cells during development in organ culture. *Int Immunol* **28**, 513-518 (2016).

75. Tian, L., Lu, L., Yuan, Z., Lamb, J.R. & Tam, P.K. Acceleration of apoptosis in CD4+CD8+ thymocytes by rapamycin accompanied by increased CD4+CD25+ T cells in the periphery. *Transplantation* **77**, 183-189 (2004).

76. Nedjic, J., Aichinger, M., Emmerich, J., Mizushima, N. & Klein, L. Autophagy in thymic epithelium shapes the T-cell repertoire and is essential for tolerance. *Nature* **455**, 396-400 (2008).

77. Holz, M.K. & Blenis, J. Identification of S6 kinase 1 as a novel mammalian target of rapamycin (mTOR)-phosphorylating kinase. *J Biol Chem* **280**, 26089-26093 (2005).

78. Nikolich-Zugich, J. *et al.* SARS-CoV-2 and COVID-19 in older adults: what we may expect regarding pathogenesis, immune responses, and outcomes. *Geroscience* **42**, 505-514 (2020).

79. Yager, E.J. *et al.* Age-associated decline in T cell repertoire diversity leads to holes in the repertoire and impaired immunity to influenza virus. *The Journal of experimental medicine* **205**, 711-723 (2008).

80. Elfaki, Y. *et al.* Influenza A virus-induced thymus atrophy differentially affects dynamics of conventional and regulatory T-cell development in mice. *Eur J Immunol* **51**, 1166-1181 (2021).

81. Onodera, T. *et al.* Thymic atrophy in type 2 reovirus infected mice: immunosuppression and effects of thymic hormone. Thymic atrophy caused by reo-2. *Thymus* **18**, 95-109 (1991).

82. Savino, W. The thymus is a common target organ in infectious diseases. *PLoS Pathog* **2**, e62 (2006).

83. Callahan, J.E., Kappler, J.W. & Marrack, P. Unexpected expansions of CD8-bearing cells in old mice. *J Immunol* **151**, 6657-6669 (1993).

84. Posnett, D.N. *et al.* Oligoclonal expansions of antigen-specific CD8+ T cells in aged mice. *Ann N Y Acad Sci* **987**, 274-279 (2003).

85. Messaoudi, I., Lemaoult, J., Guevara-Patino, J.A., Metzner, B.M. & Nikolich-Zugich, J. Age-related CD8 T cell clonal expansions constrict CD8 T cell repertoire and have the potential to impair immune defense. *The Journal of experimental medicine* **200**, 1347-1358 (2004).

86. Breed, E.R., Watanabe, M. & Hogquist, K.A. Measuring Thymic Clonal Deletion at the Population Level. *J Immunol* **202**, 3226-3233 (2019).

87. Semwal, M.K. *et al.* Redox status regulates autophagy in thymic stromal cells and promotes T cell tolerance. *Proceedings of the National Academy of Sciences of the United States of America* **119**, e2204296119 (2022).

88. Sharma, S., Dominguez, A.L. & Lustgarten, J. High accumulation of T regulatory cells prevents the activation of immune responses in aged animals. *J Immunol* **177**, 8348-8355 (2006).

89. Lages, C.S. *et al.* Functional regulatory T cells accumulate in aged hosts and promote chronic infectious disease reactivation. *J Immunol* **181**, 1835-1848 (2008).

90. Raynor, J. *et al.* IL-15 Fosters Age-Driven Regulatory T Cell Accrual in the Face of Declining IL-2 Levels. *Front Immunol* **4**, 161 (2013).

91. Thornton, A.M. *et al.* Helios(+) and Helios(-) Treg subpopulations are phenotypically and functionally distinct and express dissimilar TCR repertoires. *Eur J Immunol* **49**, 398-412 (2019).

92. Raynor, J. *et al.* IL-6 and ICOS Antagonize Bim and Promote Regulatory T Cell Accrual with Age. *J Immunol* **195**, 944-952 (2015).

93. Prockop, S.E. & Petrie, H.T. Regulation of thymus size by competition for stromal niches among early T cell progenitors. *J Immunol* **173**, 1604-1611 (2004).

94. Snippert, H.J. *et al.* Intestinal crypt homeostasis results from neutral competition between symmetrically dividing Lgr5 stem cells. *Cell* **143**, 134-144 (2010).

95. Kendall, M.D. *The Thymus gland*. Academic Press: London ; New York, 1981.

96. Majumdar, S. & Nandi, D. Thymic Atrophy: Experimental Studies and Therapeutic Interventions. *Scand J Immunol* (2017).

97. Taub, D.D. & Longo, D.L. Insights into thymic aging and regeneration. *Immunol Rev* **205**, 72-93 (2005).

98. Elsaesser, H.J. *et al.* Chronic virus infection drives CD8 T cell-mediated thymic destruction and impaired negative selection. *Proceedings of the National Academy of Sciences of the United States of America* **117**, 5420-5429 (2020).

99. Silva-Garcia, C.G. Devo-Aging: Intersections Between Development and Aging. *Geroscience* **45**, 2145-2159 (2023).

100. Zwaan, B.J. Linking development and aging. *Sci Aging Knowledge Environ* **2003**, pe32 (2003).

101. Rando, T.A. & Chang, H.Y. Aging, rejuvenation, and epigenetic reprogramming: resetting the aging clock. *Cell* **148**, 46-57 (2012).

102. Kishi, S. Using zebrafish models to explore genetic and epigenetic impacts on evolutionary developmental origins of aging. *Transl Res* **163**, 123-135 (2014).

103. Shindyapina, A.V. *et al.* Rapamycin treatment during development extends life span and health span of male mice and Daphnia magna. *Sci Adv* **8**, eabo5482 (2022).

104. Aiello, G. *et al.* Transient rapamycin treatment during developmental stage extends lifespan in Mus musculus and Drosophila melanogaster. *EMBO Rep* **23**, e55299 (2022).

105. Tu, M.P. & Tatar, M. Juvenile diet restriction and the aging and reproduction of adult Drosophila melanogaster. *Aging Cell* **2**, 327-333 (2003).

106. Lints, F.A. & Lints, C.V. Influence of preimaginal environment on fecundity and ageing in Drosophila melanogaster hybirds. I. Preimaginal population density. *Exp Gerontol* **4**, 231-244 (1969).

107. Miller, R.S.T., J. L. The Effects of Larval Crowding and Body Size on the Longevity of Adult Drosophila Melanogaster. *Ecology* **39**, 118-125 (1958).

108. Sorensen, J.G. & Loeschcke, V. Larval crowding in Drosophila melanogaster induces Hsp70 expression, and leads to increased adult longevity and adult thermal stress resistance. *J Insect Physiol* **47**, 1301-1307 (2001).

109. Zwaan, B.J., Bijlsma, R. & Hoekstra, R.F. On the developmental theory of ageing. I. starvation resistance and longevity in Drosophila melanogaster in relation to pre-adult breeding conditions. *Heredity (Edinb)* **66 (Pt 1)**, 29-39 (1991).

110. Sun, L., Sadighi Akha, A.A., Miller, R.A. & Harper, J.M. Life-span extension in mice by preweaning food restriction and by methionine restriction in middle age. *J Gerontol A Biol Sci Med Sci* **64**, 711-722 (2009).

111. Sun, L.Y. *et al.* Longevity is impacted by growth hormone action during early postnatal period. *Elife* **6** (2017).

112. Duah, M. *et al.* Thymus Degeneration and Regeneration. *Front Immunol* **12**, 706244 (2021).

113. Spadaro, O. *et al.* Caloric restriction in humans reveals immunometabolic regulators of health span. *Science* **375**, 671-677 (2022).

114. Dudakov, J.A. *et al.* Interleukin-22 drives endogenous thymic regeneration in mice. *Science* **336**, 91-95 (2012).

115. Kinsella, S. & Dudakov, J.A. When the Damage Is Done: Injury and Repair in Thymus Function. *Front Immunol* **11**, 1745 (2020).

116. Velardi, E., Dudakov, J.A. & van den Brink, M.R. Clinical strategies to enhance thymic recovery after allogeneic hematopoietic stem cell transplantation. *Immunology letters* **155**, 31-35 (2013).

117. Wertheimer, T. *et al.* Production of BMP4 by endothelial cells is crucial for endogenous thymic regeneration. *Sci Immunol* **3** (2018).

118. Kousa, A.I. *et al.* Age-related epithelial defects limit thymic function and regeneration. *Nat Immunol* **25**, 1593-1606 (2024).

119. Griffith, A.V. *et al.* Metabolic Damage and Premature Thymus Aging Caused by Stromal Catalase Deficiency. *Cell Reports* **12**, 1071-1079 (2015).

120. Liang, Z. *et al.* The Development and Survival of Thymic Epithelial Cells Require TSC1-Dependent Negative Regulation of mTORC1 Activity. *J Immunol* **207**, 2039-2050 (2021).

121. Wu, X. *et al.* Separating mitogenic and metabolic activities of fibroblast growth factor 19 (FGF19). *Proceedings of the National Academy of Sciences of the United States of America* **107**, 14158-14163 (2010).

122. Kliewer, S.A. & Mangelsdorf, D.J. A Dozen Years of Discovery: Insights into the Physiology and Pharmacology of FGF21. *Cell Metab* **29**, 246-253 (2019).

123. Kussendrager, K.D. & van Hooijdonk, A.C. Lactoperoxidase: physico-chemical properties, occurrence, mechanism of action and applications. *Br J Nutr* **84 Suppl 1**, S19-25 (2000).

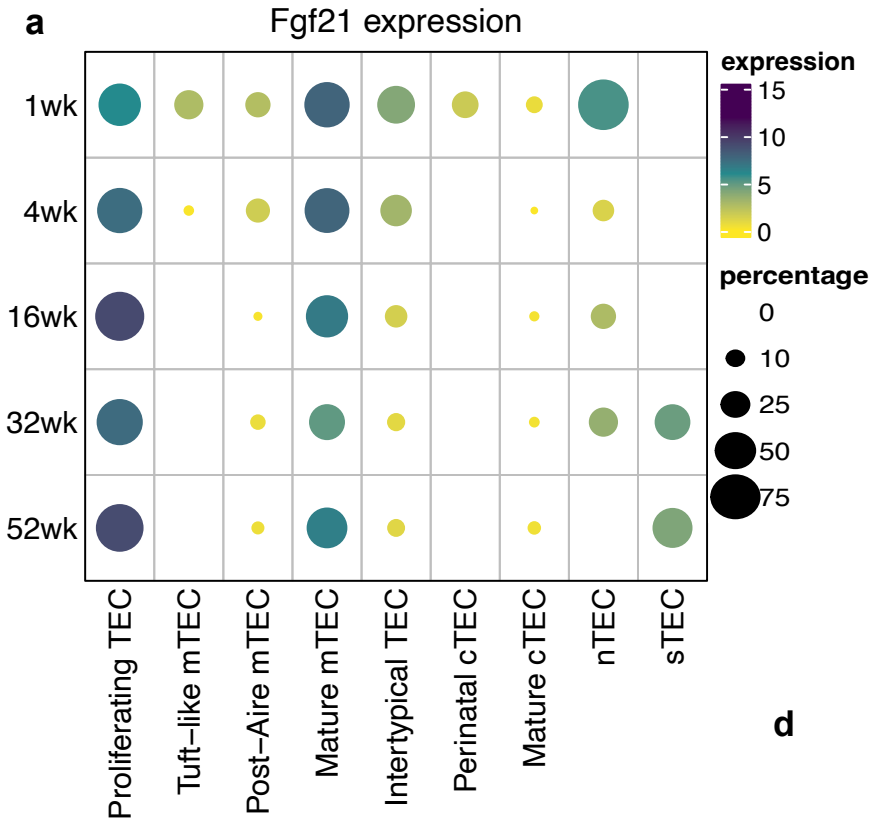
124. Bafort, F., Parisi, O., Perraudin, J.P. & Jijakli, M.H. Mode of action of lactoperoxidase as related to its antimicrobial activity: a review. *Enzyme Res* **2014**, 517164 (2014).

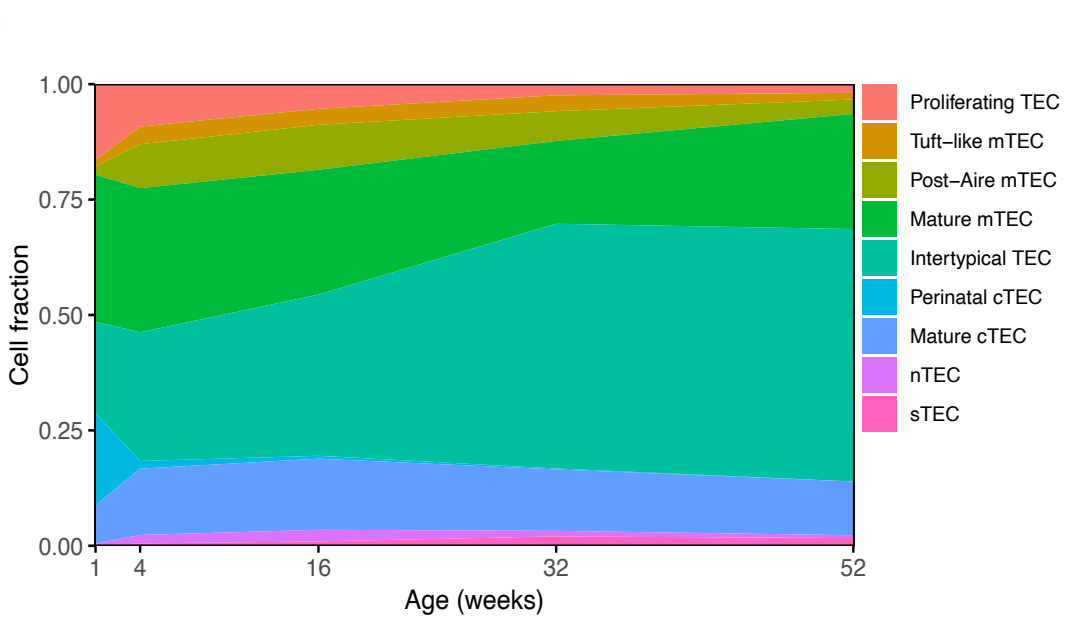
125. Magacz, M., Kedziora, K., Sapa, J. & Krzysciak, W. The Significance of Lactoperoxidase System in Oral Health: Application and Efficacy in Oral Hygiene Products. *Int J Mol Sci* **20** (2019).

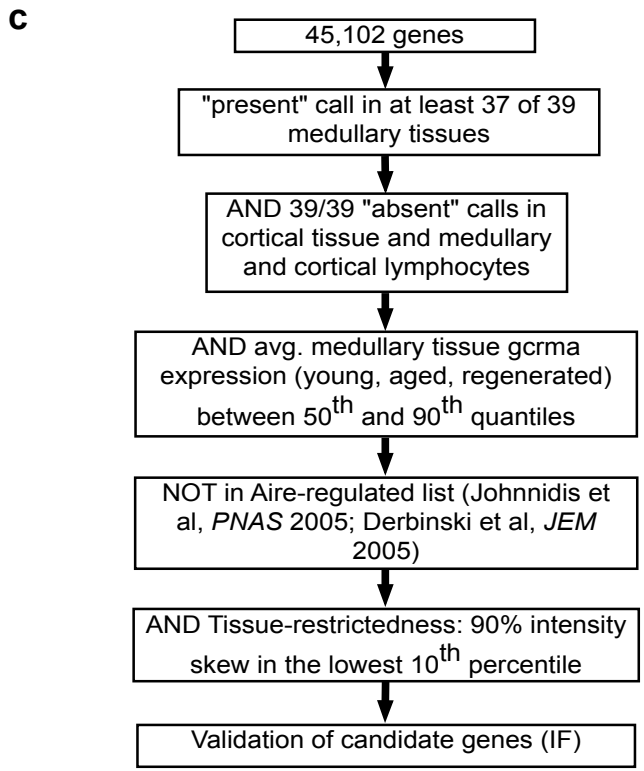
126. Oikonomou, V. *et al.* The Role of Interferon-gamma in Autoimmune Polyendocrine Syndrome Type 1. *N Engl J Med* **390**, 1873-1884 (2024).

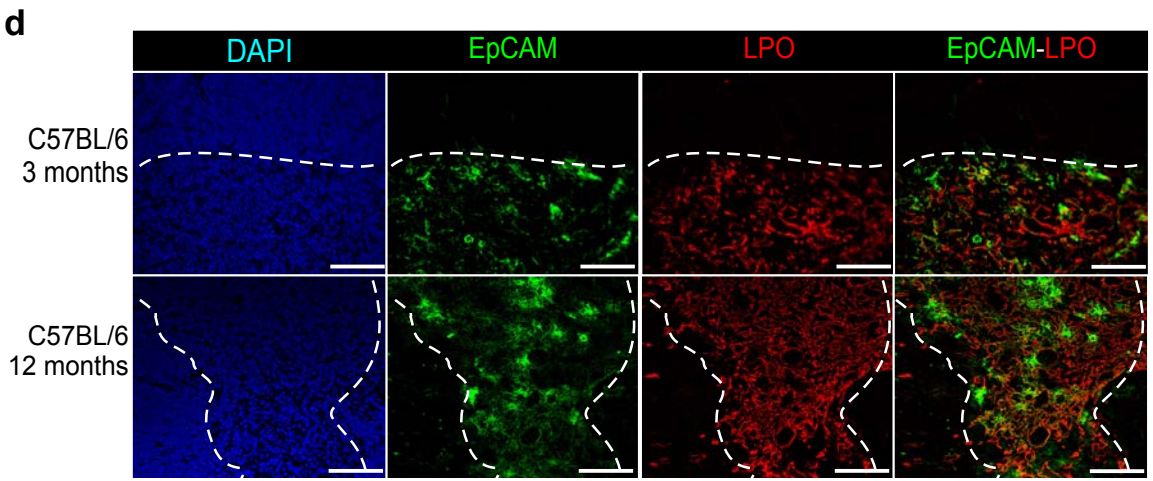
127. Martinez, R.J. *et al*. Type III interferon drives thymic B cell activation and regulatory T cell generation. *Proceedings of the National Academy of Sciences of the United States of America* **120**, e2220120120 (2023).

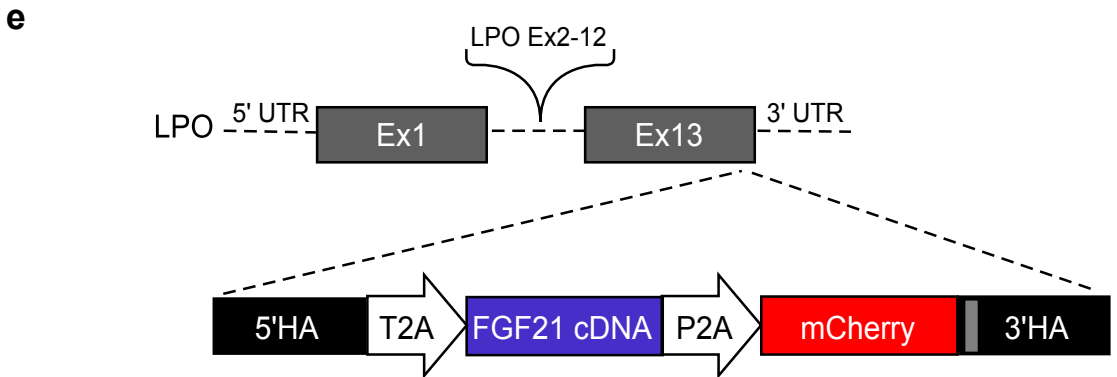
128. Yamakaze, J. & Lu, Z. Deletion of the lactoperoxidase gene causes multisystem inflammation and tumors in mice. *Sci Rep* **11**, 12429 (2021).

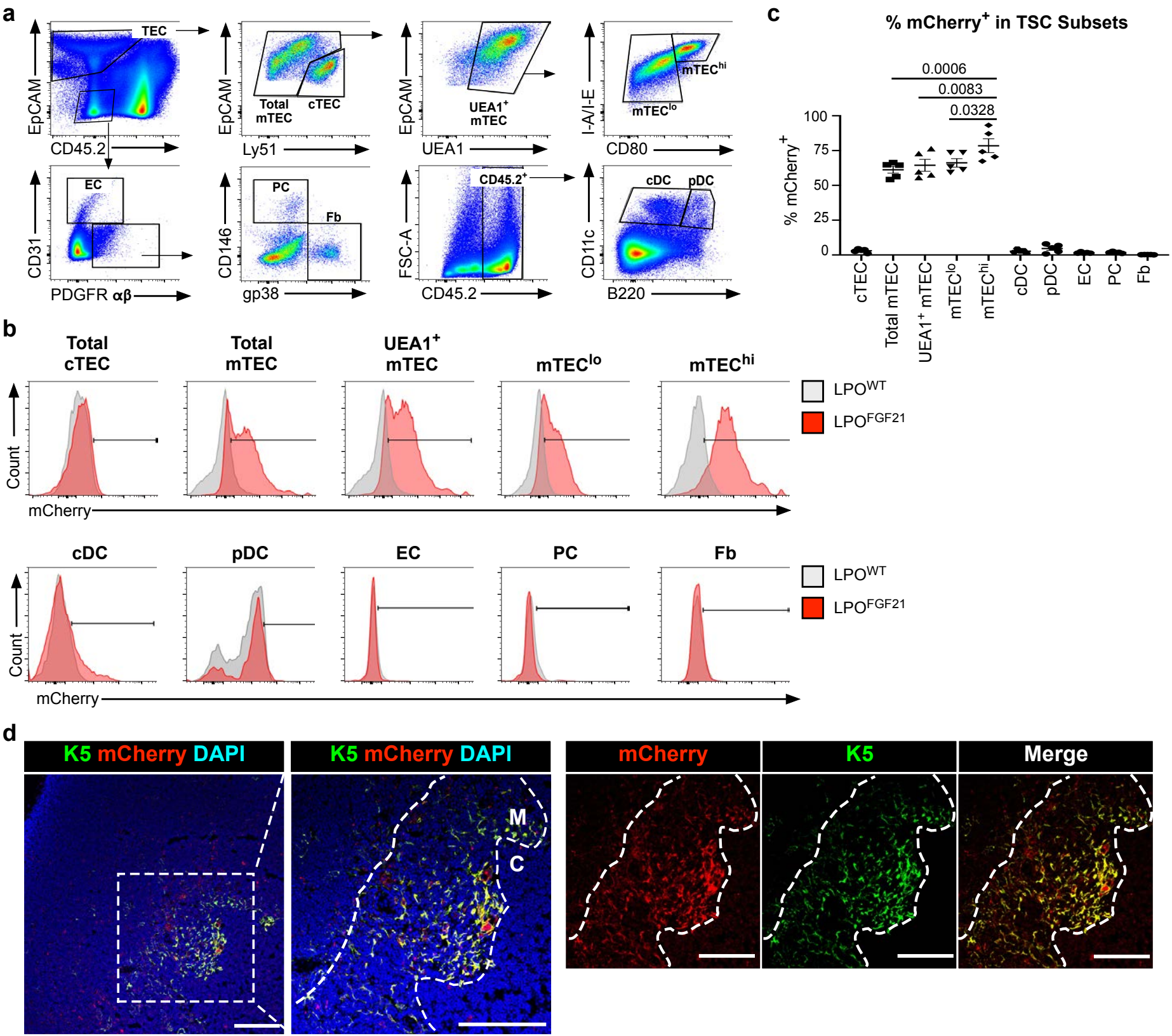

a
Fgf21 expression
1wk
4wk
16wk
32wk
52wk
Proliferating TEC
Tuft−like mTEC
Post−Aire mTEC
Mature mTEC
Intertypical TEC
Perinatal cTEC
Mature cTEC
nTEC
sTEC
expression
15
10
5
0
percentage
0
10
25
50
75

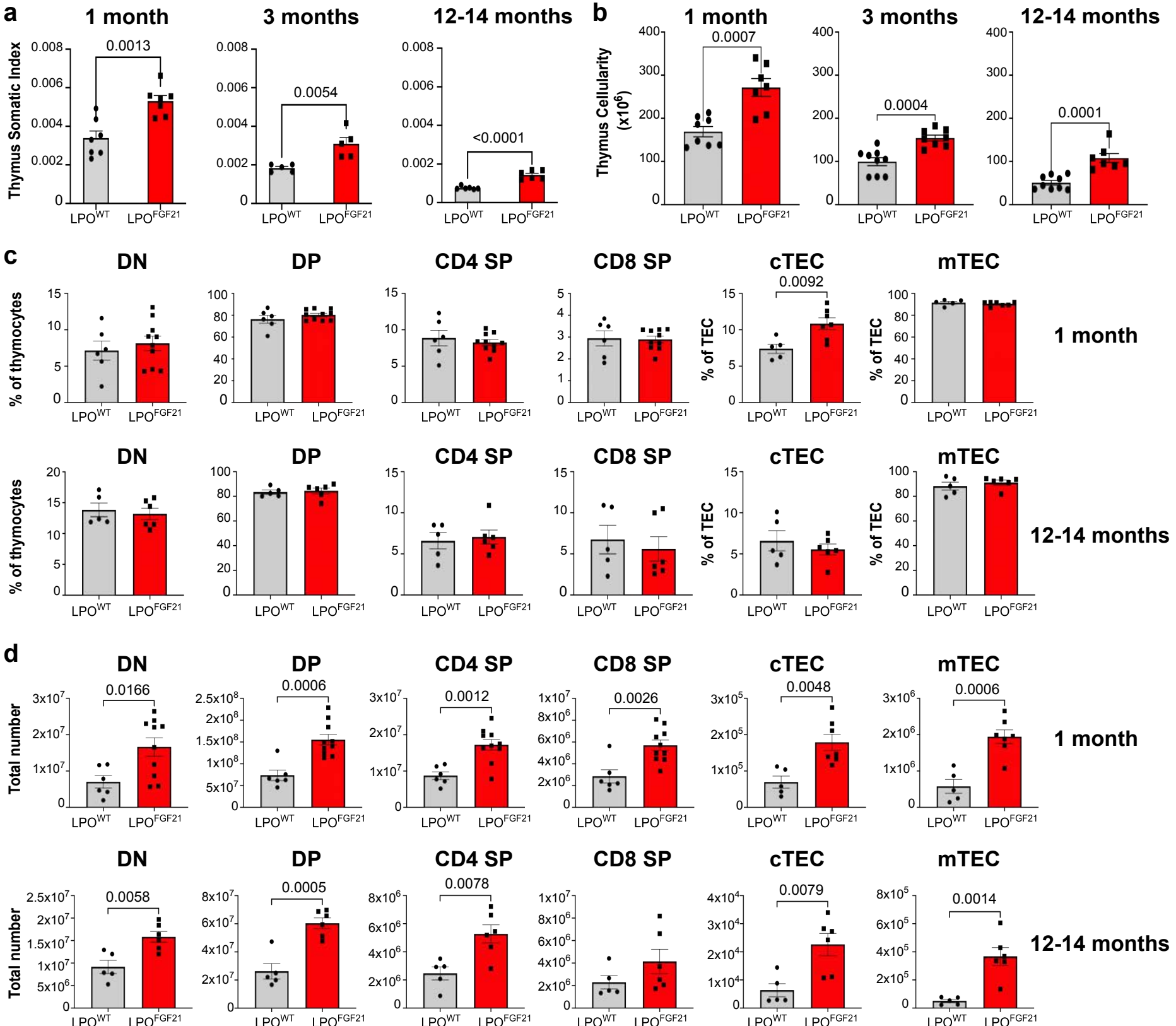

b
1.00
0.75
0.50
0.25
0.00
Cell fraction
1
4
16
32
52
Age (weeks)
Proliferating TEC
Tuft−like mTEC
Post−Aire mTEC
Mature mTEC
Intertypical TEC
Perinatal cTEC
Mature cTEC
nTEC
sTEC

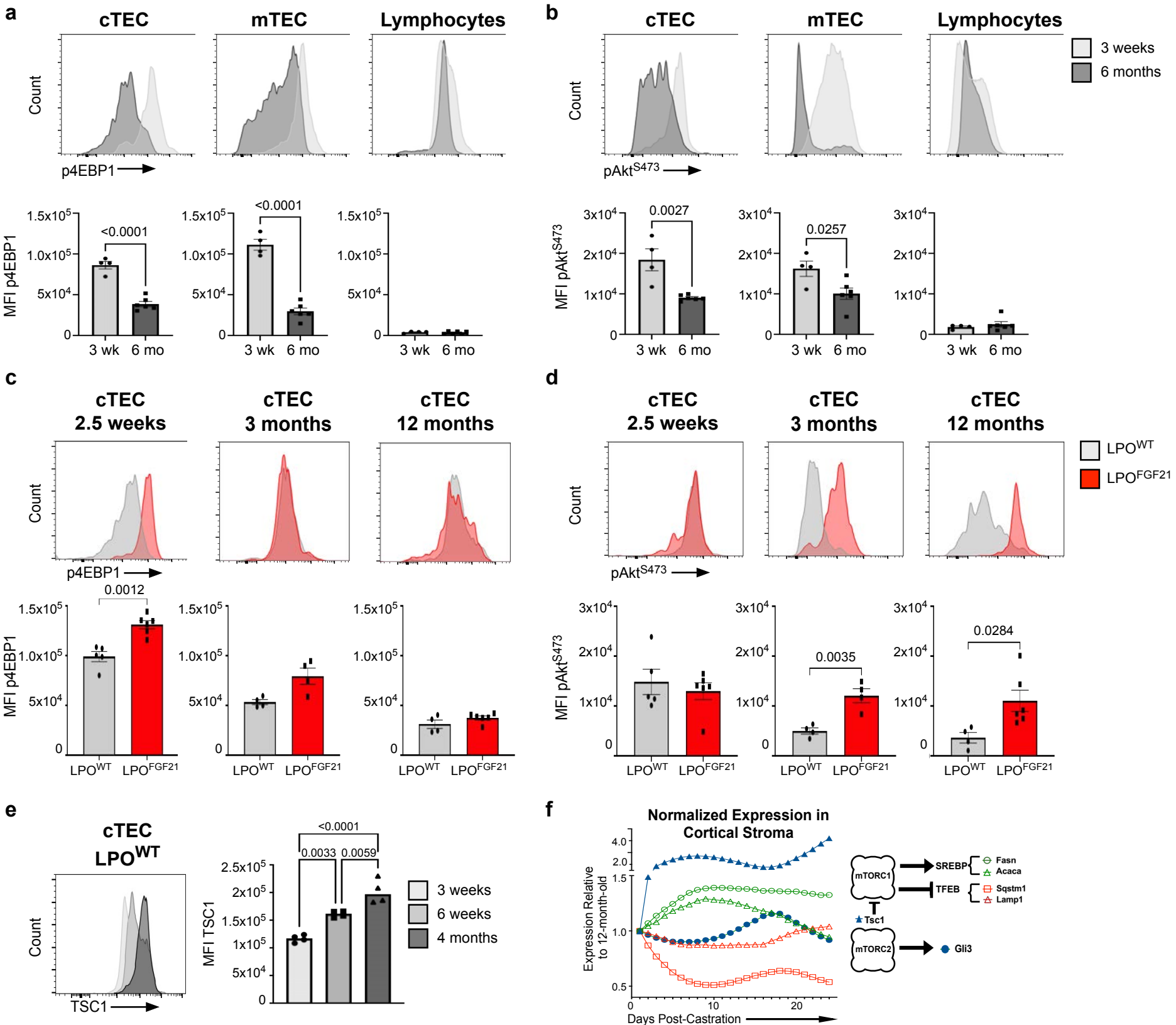

c
45,102 genes
"present" call in at least 37 of 39 medullary tissues
AND 39/39 "absent" calls in cortical tissue and medullary and cortical lymphocytes
AND avg. medullary tissue gcrma expression (young, aged, regenerated) between 50th and 90th quantiles
NOT in Aire-regulated list (Johnnidis et al, PNAS 2005; Derbinski et al, JEM 2005)
AND Tissue-restrictedness: 90% intensity skew in the lowest 10th percentile
Validation of candidate genes (IF)

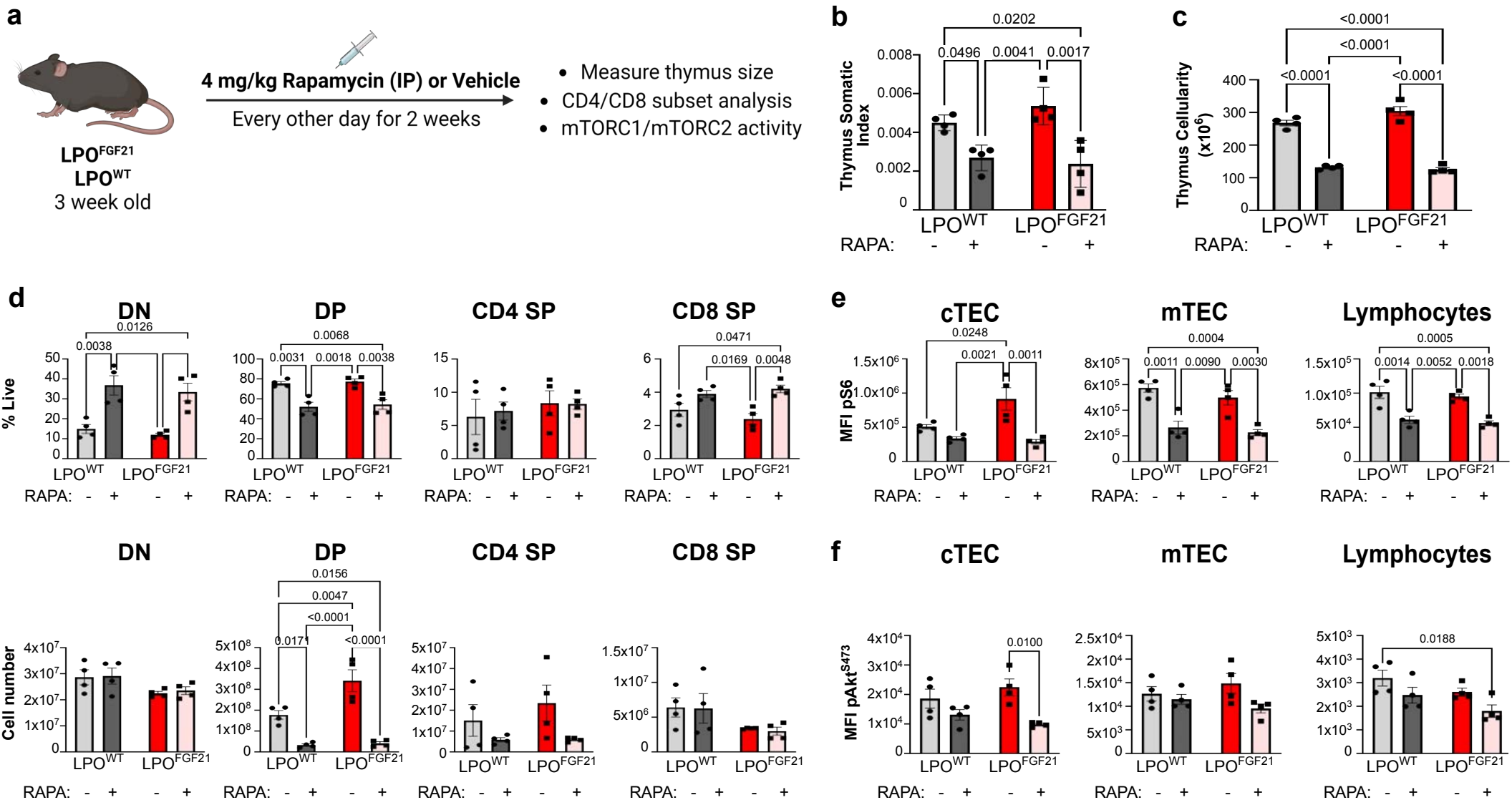

d
DAPI
EpCAM
LPO
EpCAM-LPO
C57BL/6
3 months
C57BL/6
12 months

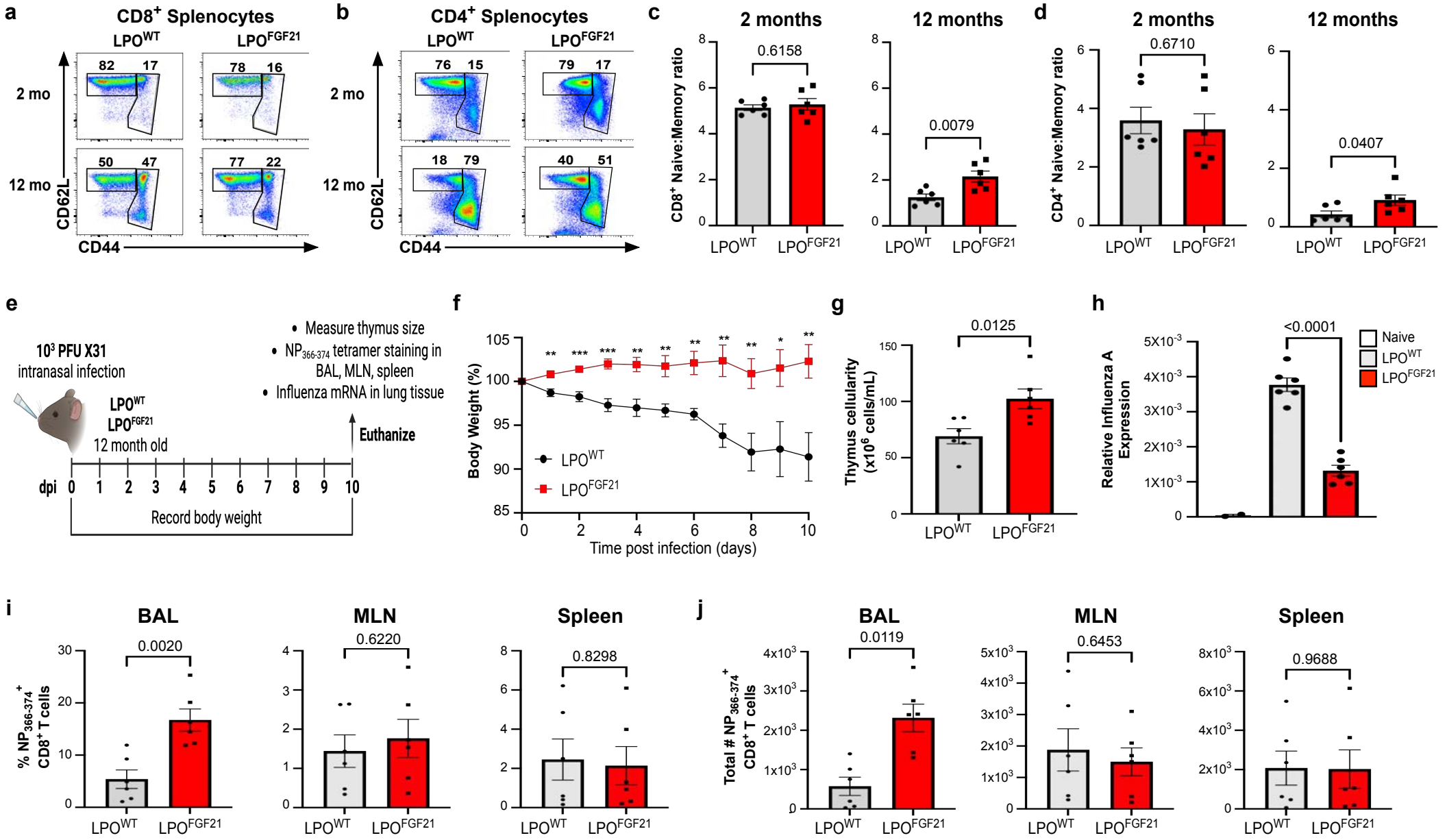

e
LPO Ex2-12
LPO
5' UTR
Ex1
Ex13
3' UTR
5'HA
T2A
FGF21 cDNA
P2A
mCherry
3'HA

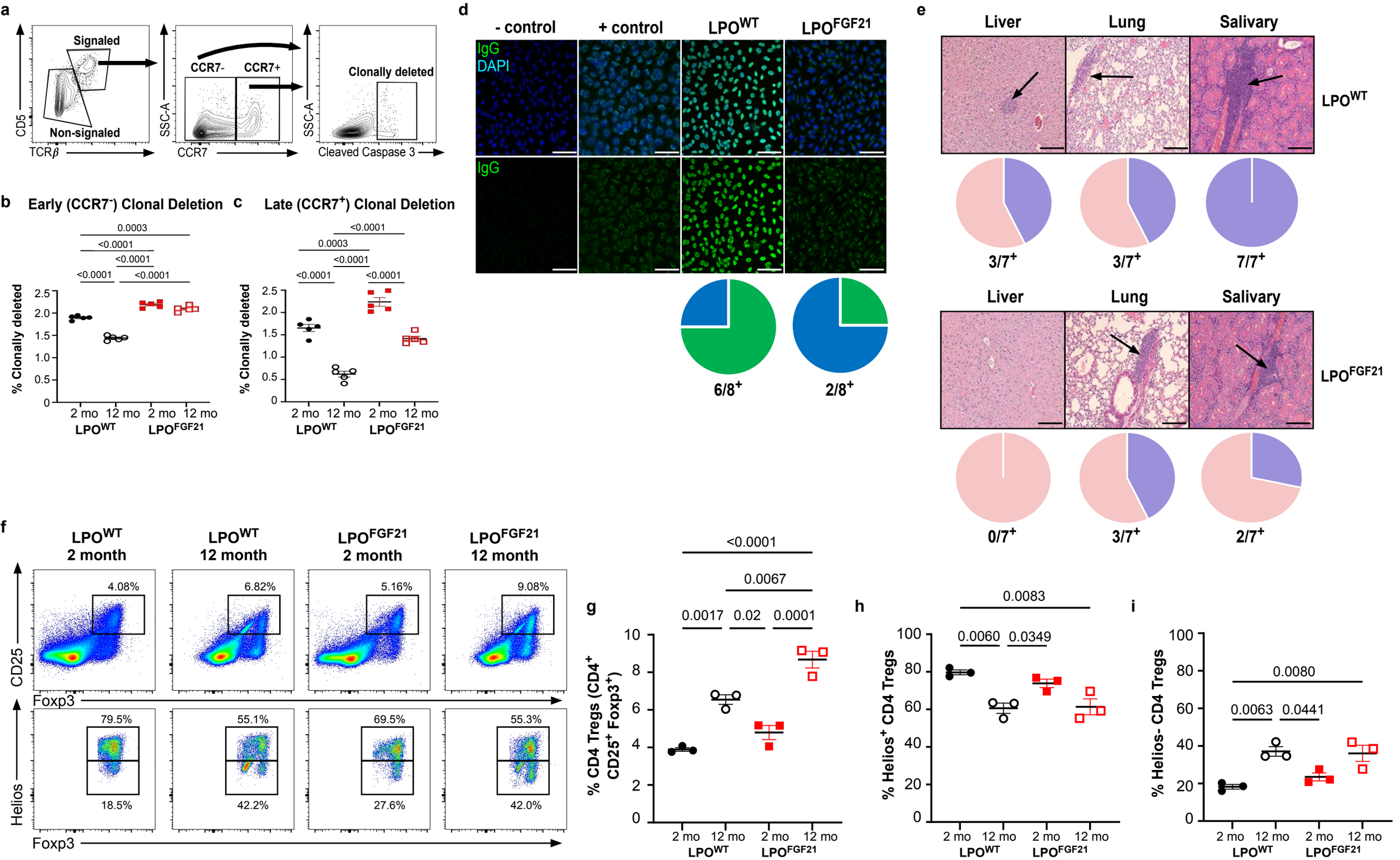

a
TEC
EpCAM
CD45.2
Total mTEC
cTEC
Ly51
UEA1+ mTEC
UEA1
mTEChi
mTEClo
I-A/I-E
CD80
EC
CD31
PDGFR αβ
PC
Fb
CD146
gp38
CD45.2+
FSC-A
cDC
pDC
CD11c
B220
b
Total cTEC
Total mTEC
UEA1+ mTEC
mTEClo
mTEChi
LPOWT
LPOFGF21
Count
mCherry
cDC
pDC
EC
PC
Fb
c
% mCherry+ in TSC Subsets
0.0006
0.0083
0.0328
% mCherry+
100
75
50
25
0
cTEC
Total mTEC
UEA1+ mTEC
mTEClo
mTEChi
cDC
pDC
EC
PC
Fb
d
K5 mCherry DAPI
K5 mCherry DAPI
M
C
mCherry
K5
Merge

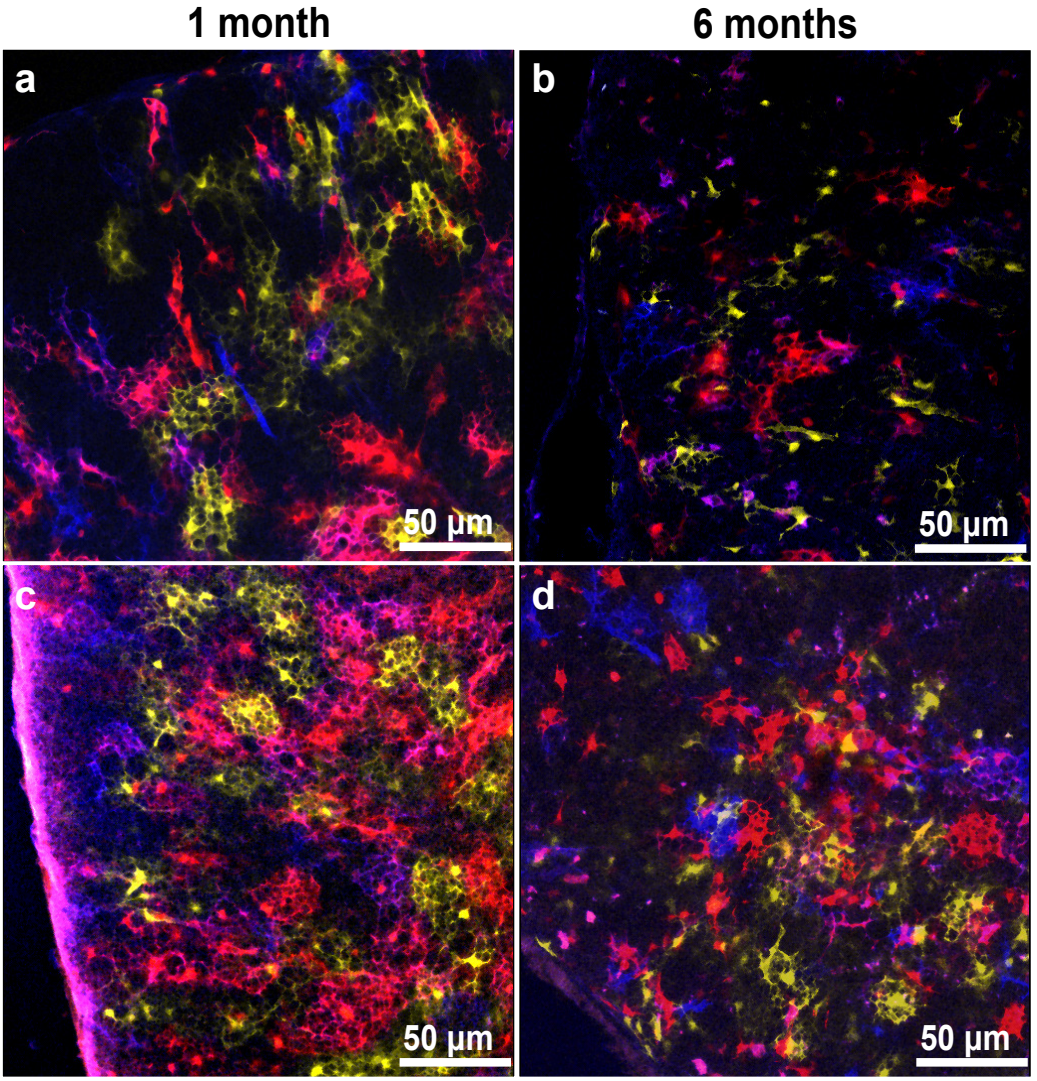

a
1 month
3 months
12-14 months
Thymus Somatic Index
0.0013
0.0054
<0.0001
b
Thymus Cellularity (x10^6)
0.0007
0.0004
0.0001
c
DN
DP
CD4 SP
CD8 SP
cTEC
mTEC
% of thymocytes
% of TEC
0.0092
1 month
12-14 months
d
Total number
0.0166
0.0006
0.0012
0.0026
0.0048
0.0006
0.0058
0.0005
0.0078
0.0079
0.0014
LPO^WT
LPO^FGF21

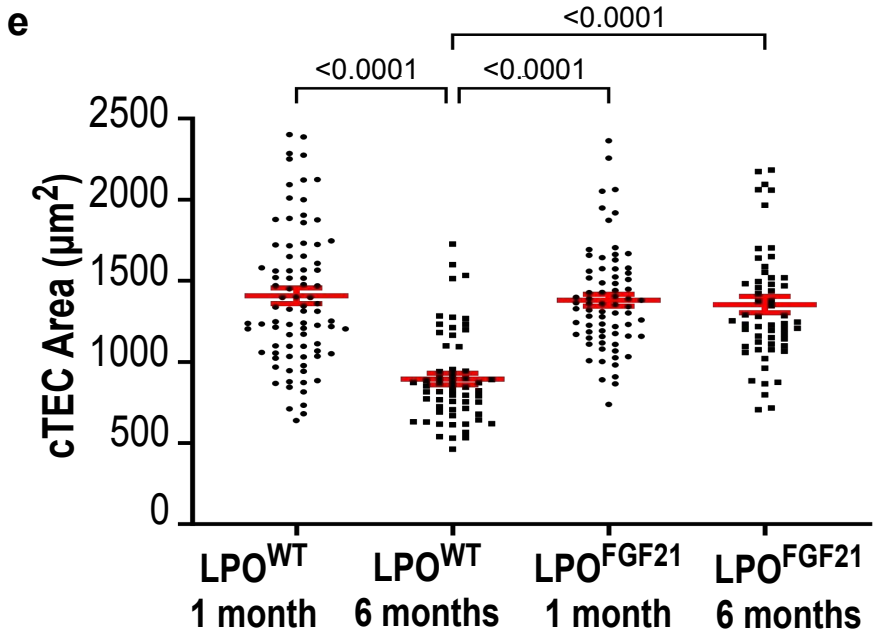

a
cTEC
mTEC
Lymphocytes
Count
p4EBP1
MFI p4EBP1
<0.0001
<0.0001
3 wk
6 mo
b
cTEC
mTEC
Lymphocytes
3 weeks
6 months
Count
pAkt^S473
MFI pAkt^S473
0.0027
0.0257
3 wk
6 mo
c
cTEC 2.5 weeks
cTEC 3 months
cTEC 12 months
Count
p4EBP1
MFI p4EBP1
0.0012
LPO^WT
LPO^FGF21
d
cTEC 2.5 weeks
cTEC 3 months
cTEC 12 months
LPO^WT
LPO^FGF21
Count
pAkt^S473
MFI pAkt^S473
0.0035
0.0284
e
cTEC LPO^WT
Count
TSC1
MFI TSC1
<0.0001
0.0033
0.0059
3 weeks
6 weeks
4 months
f
Normalized Expression in Cortical Stroma
Expression Relative to 12-month-old
Days Post-Castration
mTORC1
SREBP
Fasn
Acaca
TFEB
Sqstm1
Lamp1
Tsc1
mTORC2
Gli3

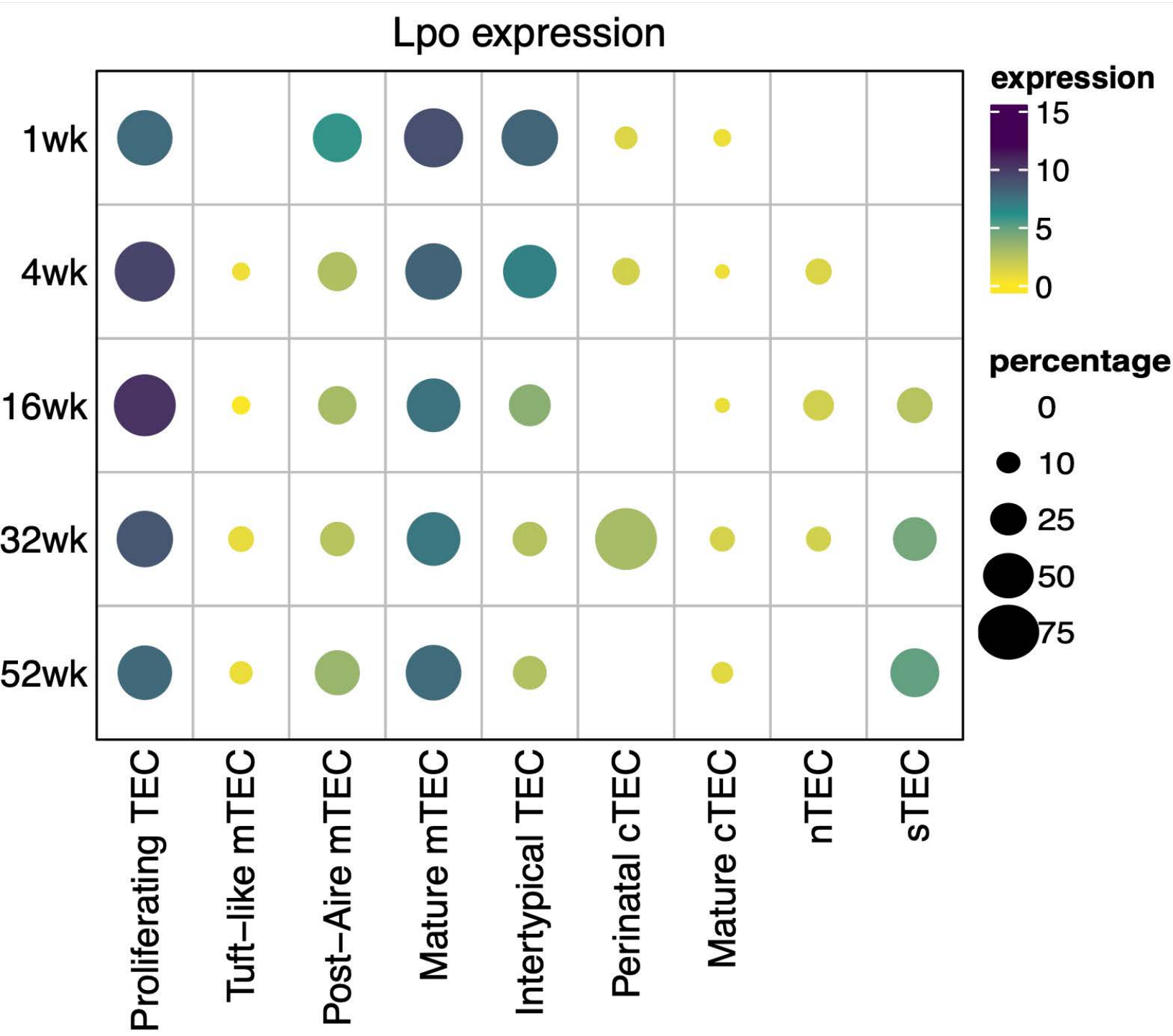

a
LPO^FGF21
LPO^WT
3 week old
4 mg/kg Rapamycin (IP) or Vehicle
Every other day for 2 weeks
Measure thymus size
CD4/CD8 subset analysis
mTORC1/mTORC2 activity
b
Thymus Somatic Index
0.0202
0.0496
0.0041
0.0017
LPO^WT
LPO^FGF21
RAPA: - + - +
c
Thymus Cellularity (x10^6)
<0.0001
<0.0001
<0.0001
<0.0001
LPO^WT
LPO^FGF21
RAPA: - + - +
d
% Live
DN
0.0126
0.0038
DP
0.0068
0.0031
0.0018
0.0038
CD4 SP
CD8 SP
0.0471
0.0169
0.0048
LPO^WT
LPO^FGF21
RAPA: - + - +
e
MFI pS6
cTEC
0.0248
0.0021
0.0011
mTEC
0.0004
0.0011
0.0090
0.0030
Lymphocytes
0.0005
0.0014
0.0052
0.0018
LPO^WT
LPO^FGF21
RAPA: - + - +
Cell number
DN
DP
0.0156
0.0047
<0.0001
0.0171
<0.0001
CD4 SP
CD8 SP
LPO^WT
LPO^FGF21
RAPA: - + - +
f
MFI pAkt^S473
cTEC
0.0100
mTEC
Lymphocytes
0.0188
LPO^WT
LPO^FGF21
RAPA: - + - +


a
CD8+ Splenocytes
LPOWT
LPOFGF21
2 mo
12 mo
82
17
78
16
50
47
77
22
CD62L
CD44
b
CD4+ Splenocytes
LPOWT
LPOFGF21
2 mo
12 mo
76
15
79
17
18
79
40
51
CD62L
CD44
c
2 months
12 months
CD8+ Naive:Memory ratio
0.6158
0.0079
LPOWT
LPOFGF21
d
2 months
12 months
CD4+ Naive:Memory ratio
0.6710
0.0407
LPOWT
LPOFGF21
e
10³ PFU X31
intranasal infection
LPOWT
LPOFGF21
12 month old
• Measure thymus size
• NP366-374 tetramer staining in BAL, MLN, spleen
• Influenza mRNA in lung tissue
Euthanize
dpi 0 1 2 3 4 5 6 7 8 9 10
Record body weight
f
Body Weight (%)
LPOWT
LPOFGF21
Time post infection (days)
g
Thymus cellularity (x10⁶ cells/mL)
0.0125
LPOWT
LPOFGF21
h
Relative Influenza A Expression
<0.0001
Naive
LPOWT
LPOFGF21
i
BAL
MLN
Spleen
% NP366-374+ CD8+ T cells
0.0020
0.6220
0.8298
LPOWT
LPOFGF21
j
BAL
MLN
Spleen
Total # NP366-374+ CD8+ T cells
0.0119
0.6453
0.9688
LPOWT
LPOFGF21

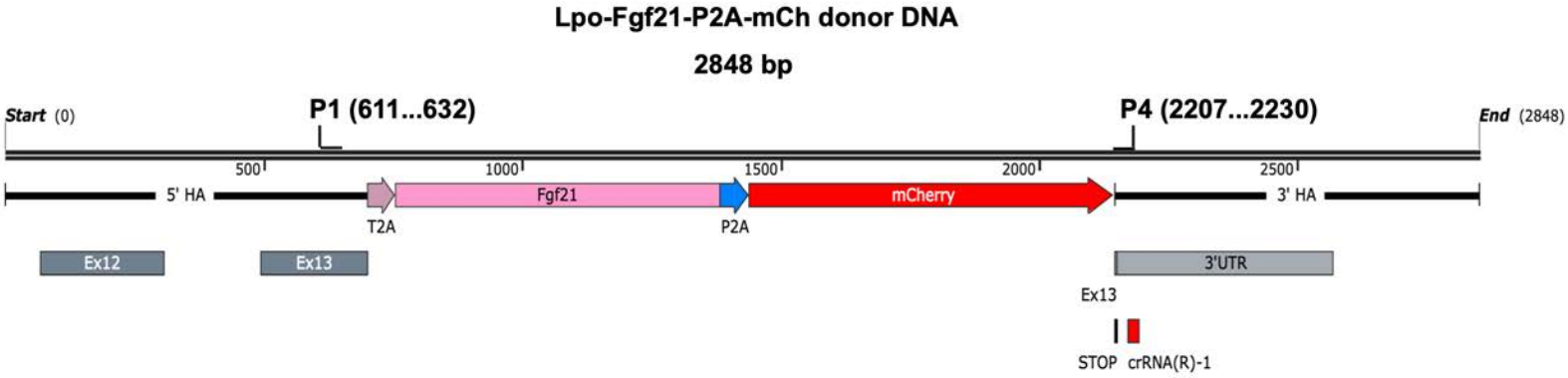

a
Signaled
Non-signaled
CD5
TCRβ
CCR7-
CCR7+
SSC-A
CCR7
Clonally deleted
Cleaved Caspase 3
b
Early (CCR7-) Clonal Deletion
% Clonally deleted
2 mo
12 mo
LPOWT
LPOFGF21
c
Late (CCR7+) Clonal Deletion
d
- control
+ control
LPOWT
LPOFGF21
IgG
DAPI
6/8+
2/8+
e
Liver
Lung
Salivary
3/7+
7/7+
0/7+
f
LPOWT 2 month
LPOWT 12 month
LPOFGF21 2 month
LPOFGF21 12 month
CD25
Foxp3
Helios
4.08%
6.82%
5.16%
9.08%
79.5%
18.5%
55.1%
42.2%
69.5%
27.6%
55.3%
42.0%
g
% CD4 Tregs (CD4+ CD25+ Foxp3+)
h
% Helios+ CD4 Tregs
i
% Helios- CD4 Tregs


1 month
6 months
a
b
c
d
50 µm
50 µm
50 µm
50 µm
LPO^WT
LPO^FGF21


e
<0.0001
<0.0001
<0.0001
cTEC Area (µm²)
2500
2000
1500
1000
500
0
LPO^WT 1 month
LPO^WT 6 months
LPO^FGF21 1 month
LPO^FGF21 6 months


Lpo expression
1wk
4wk
16wk
32wk
52wk
Proliferating TEC
Tuft−like mTEC
Post−Aire mTEC
Mature mTEC
Intertypical TEC
Perinatal cTEC
Mature cTEC
nTEC
sTEC
expression
15
10
5
0
percentage
0
10
25
50
75

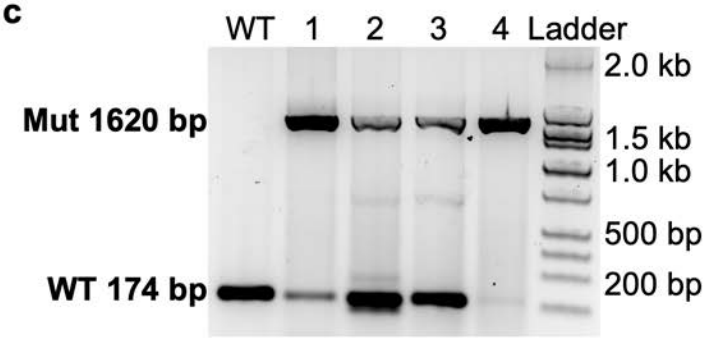
a

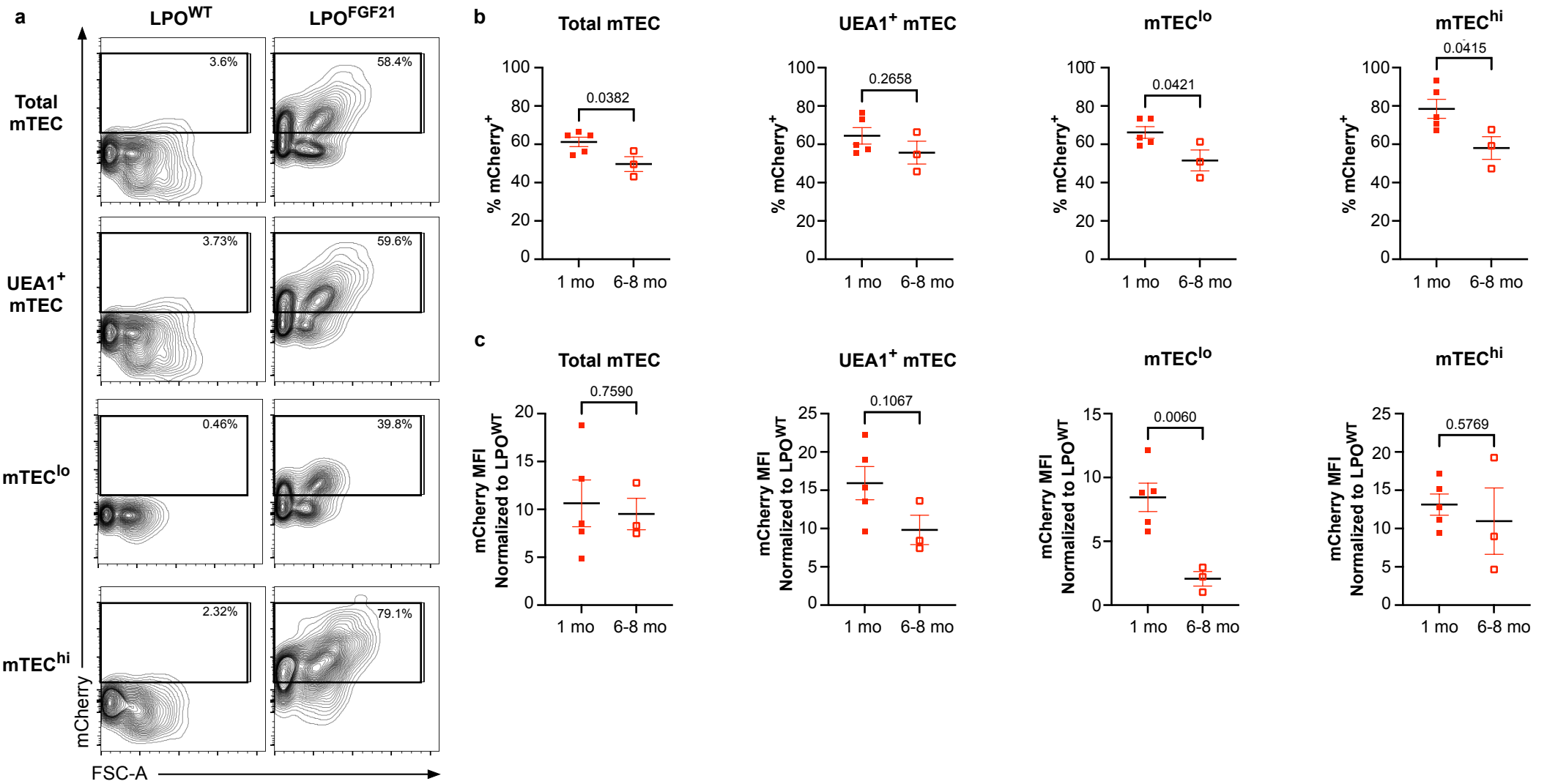


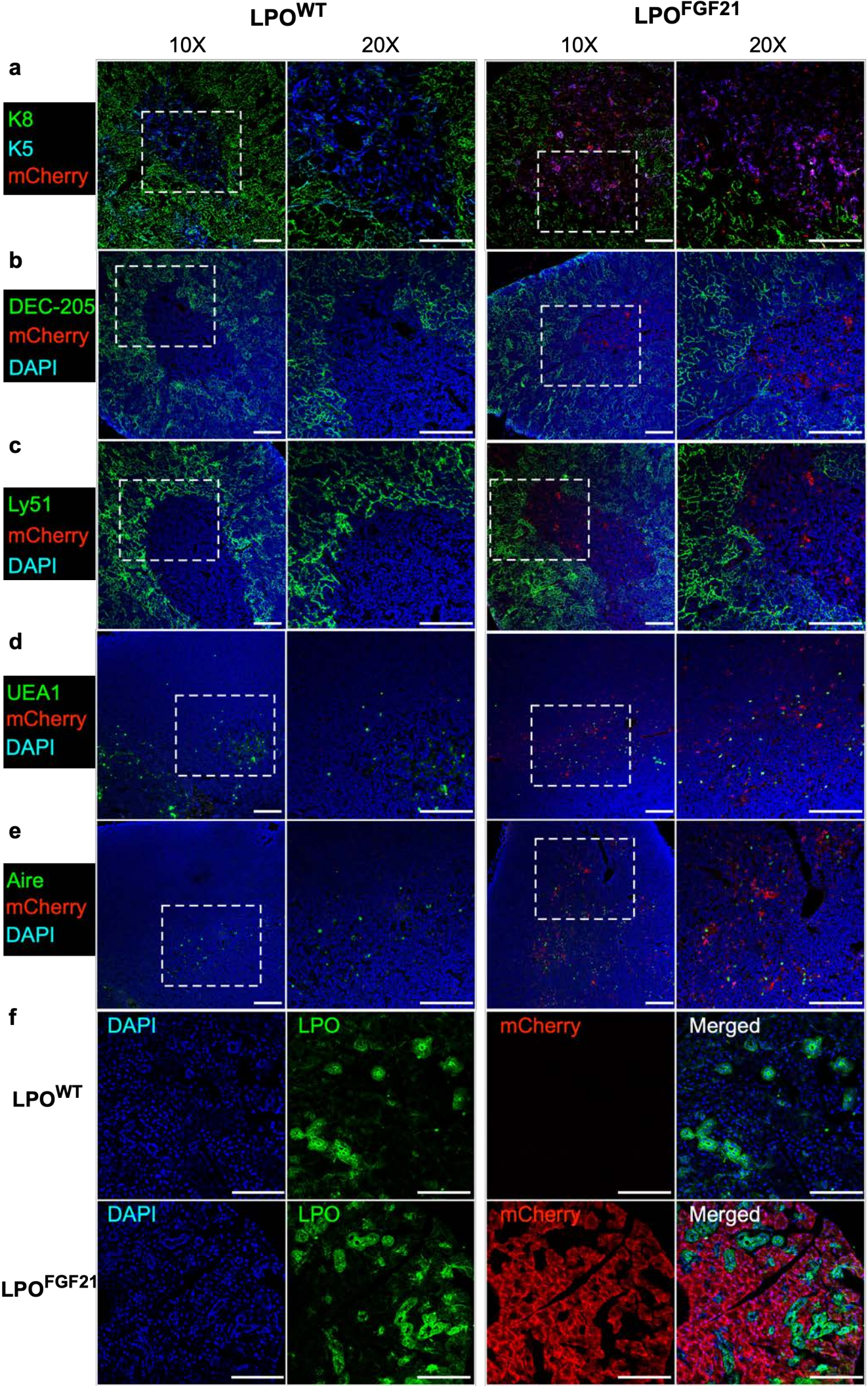
b

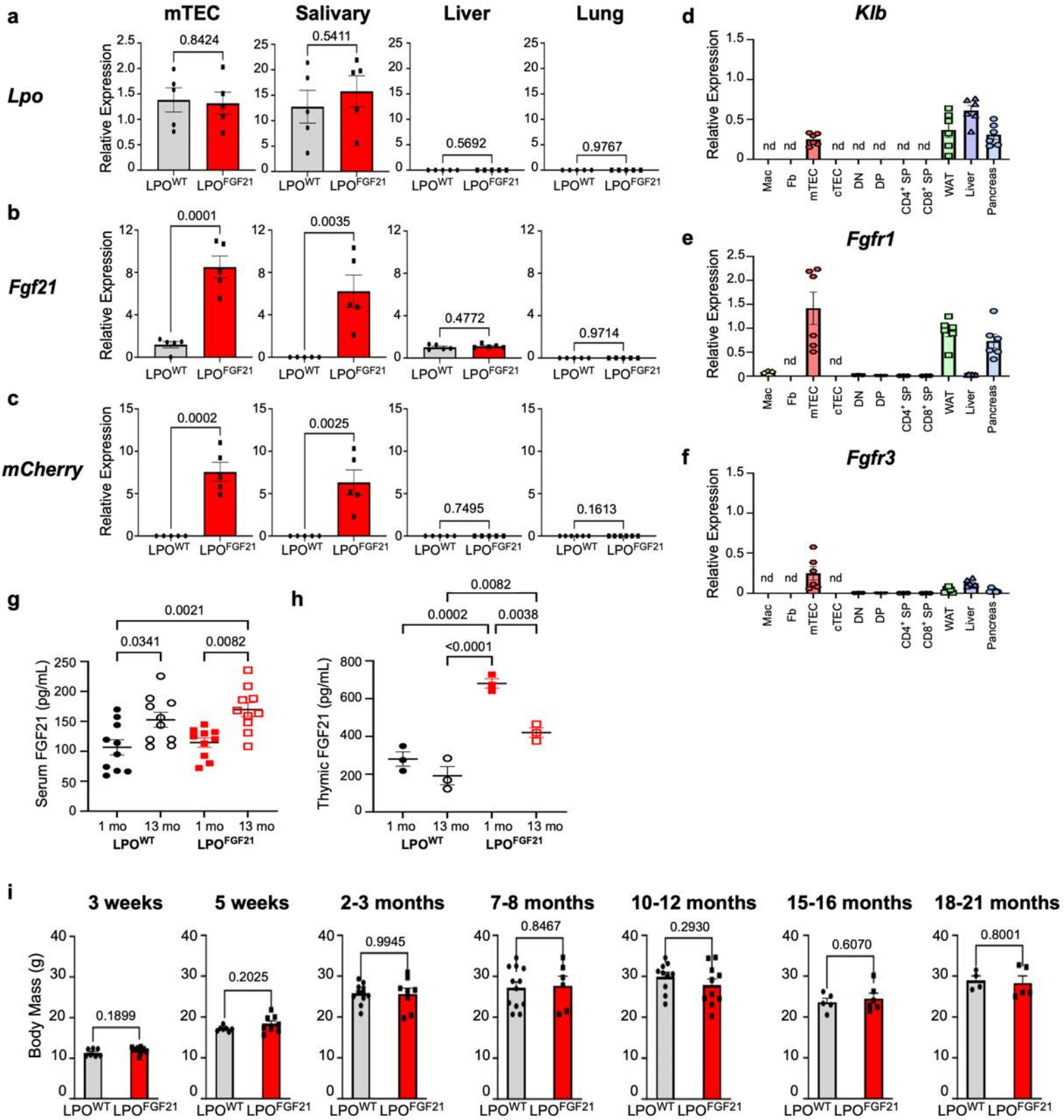
Primer sequence	
P1	5' CTGGCATCGACAAGGTCCCAC 3'
P4	5' GGAGTAGGTCACTGGAACTGTTTG 3'
Expected size	
G1 + G4	1620bp (mut) / 174 bp (WT)

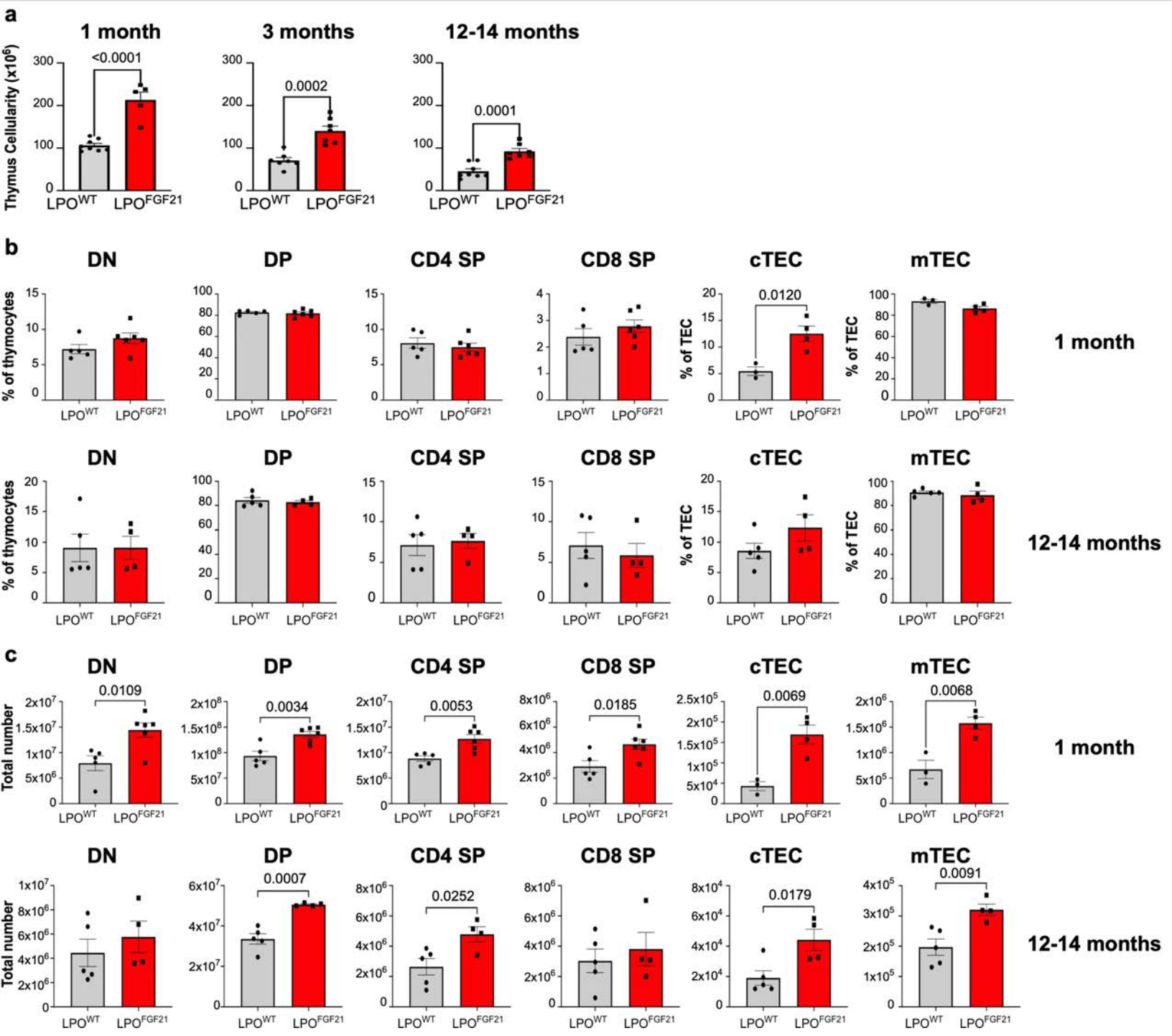
c

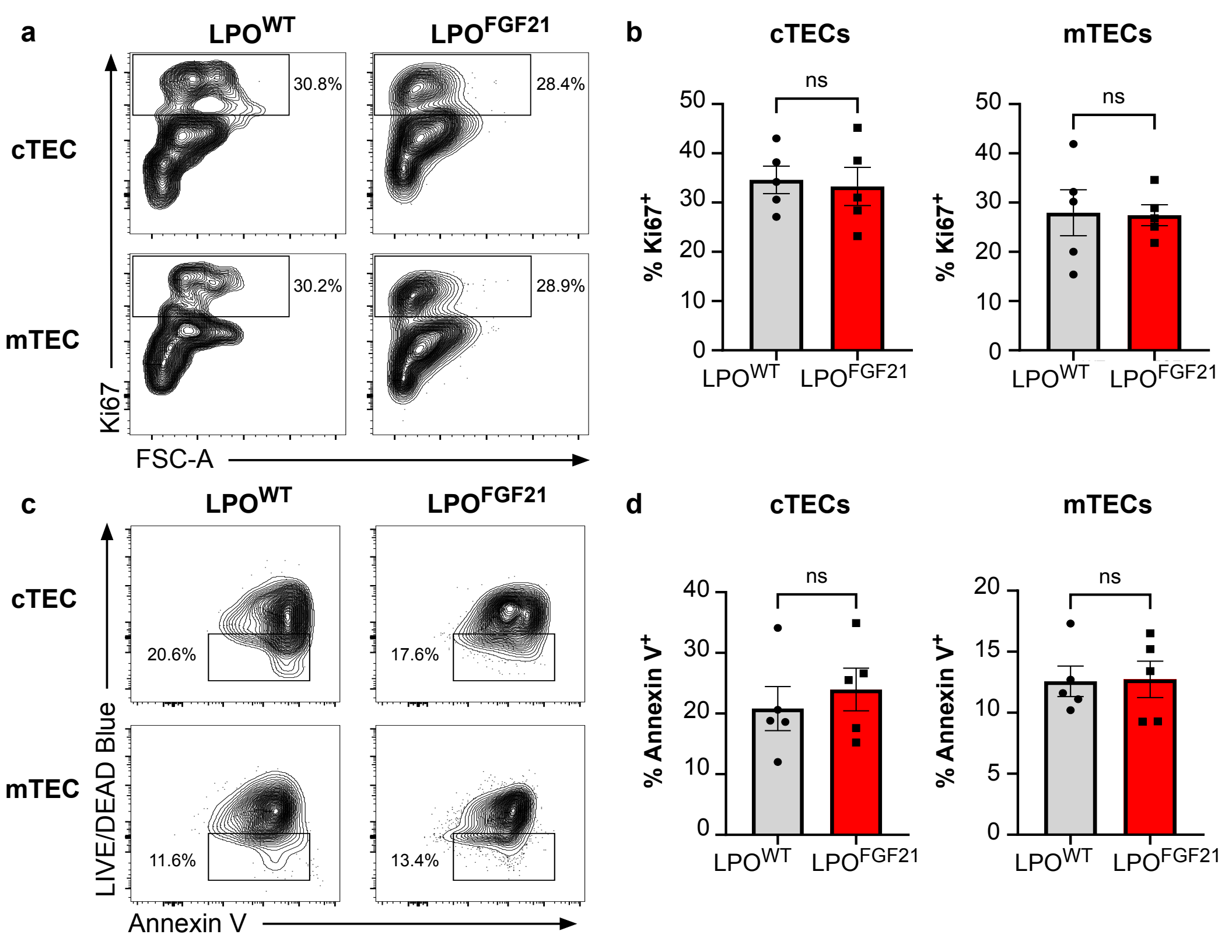


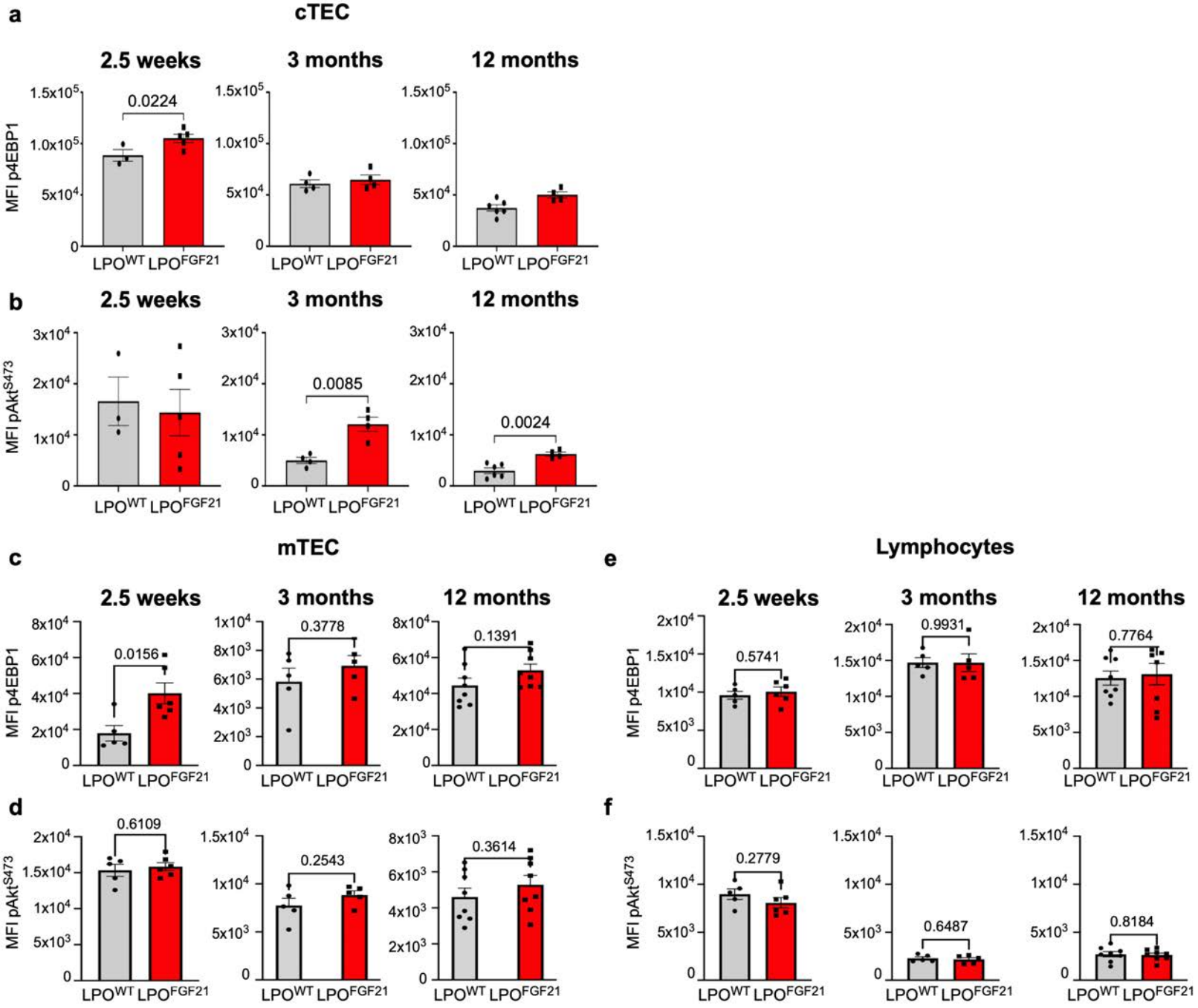

a
LPO^WT
LPO^FGF21
Total mTEC
UEA1+ mTEC
mTEClo
mTEChi
3.6%
58.4%
3.73%
59.6%
0.46%
39.8%
2.32%
79.1%
mCherry
FSC-A
b
Total mTEC
UEA1+ mTEC
mTEClo
mTEChi
% mCherry+
0.0382
0.2658
0.0421
0.0415
1 mo
6-8 mo
c
mCherry MFI Normalized to LPOWT
0.7590
0.1067
0.0060
0.5769

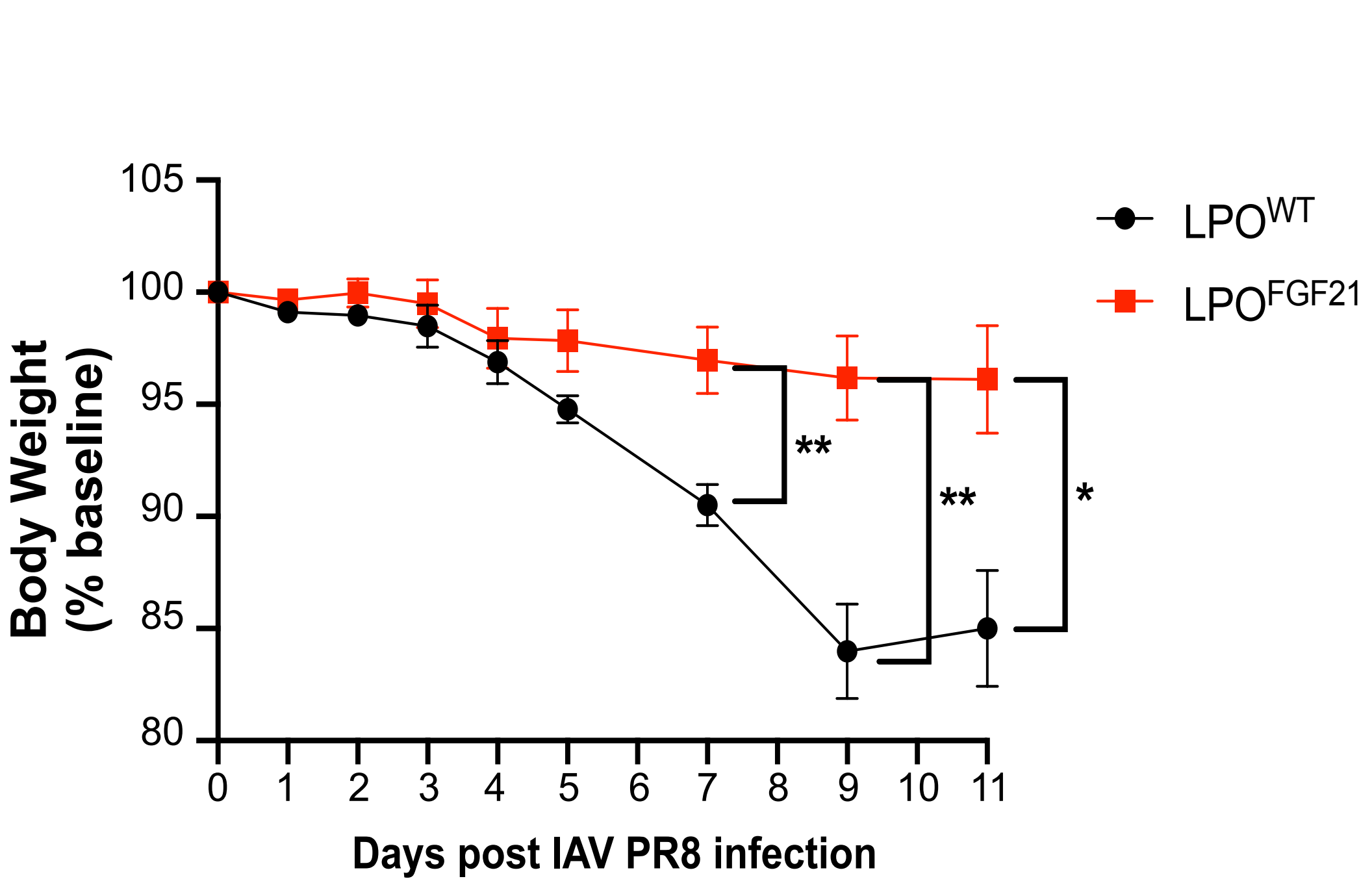

LPO^WT
LPO^FGF21
10X
20X
10X
20X
a
K8
K5
mCherry
b
DEC-205
mCherry
DAPI
c
Ly51
mCherry
DAPI
d
UEA1
mCherry
DAPI
e
Aire
mCherry
DAPI
f
DAPI
LPO
mCherry
Merged
LPO^WT
DAPI
LPO
mCherry
Merged
LPO^FGF21

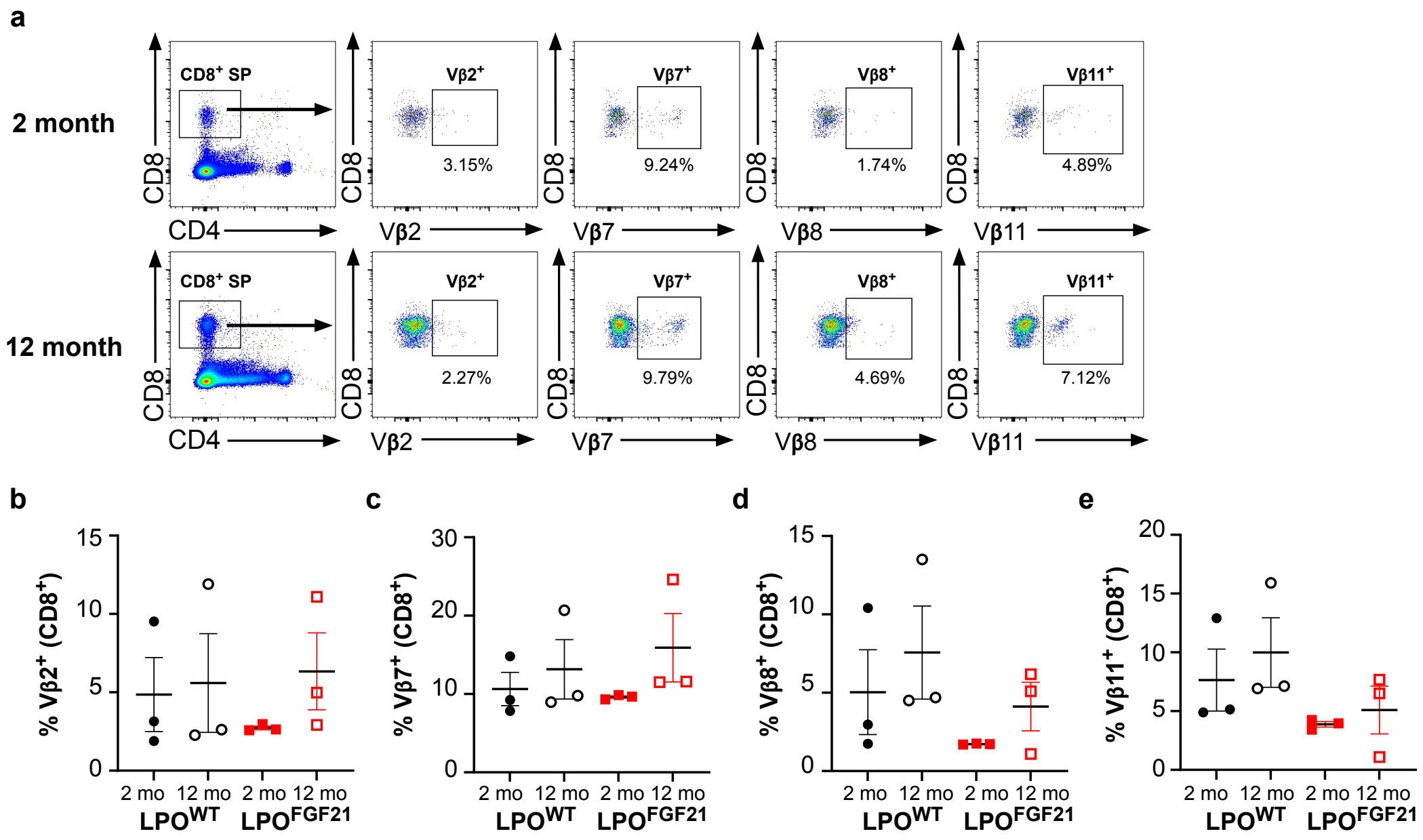

a
mTEC
Salivary
Liver
Lung
Lpo
Relative Expression
0.8424
0.5411
0.5692
0.9767
LPOWT
LPOFGF21
b
Fgf21
0.0001
0.0035
0.4772
0.9714
c
mCherry
0.0002
0.0025
0.7495
0.1613
d
Klb
e
Fgfr1
f
Fgfr3
nd
Mac
Fb
mTEC
cTEC
DN
DP
CD4+ SP
CD8+ SP
WAT
Liver
Pancreas
g
Serum FGF21 (pg/mL)
0.0021
0.0341
0.0082
1 mo
13 mo
h
Thymic FGF21 (pg/mL)
0.0082
0.0002
0.0038
<0.0001
i
3 weeks
5 weeks
2-3 months
7-8 months
10-12 months
15-16 months
18-21 months
Body Mass (g)
0.1899
0.2025
0.9945
0.8467
0.2930
0.6070
0.8001


a
1 month
3 months
12-14 months
Thymus Cellularity (x10^6)
<0.0001
0.0002
0.0001
LPO^WT
LPO^FGF21
b
DN
DP
CD4 SP
CD8 SP
cTEC
mTEC
% of thymocytes
% of TEC
0.0120
1 month
12-14 months
c
Total number
0.0109
0.0034
0.0053
0.0185
0.0069
0.0068
0.0007
0.0252
0.0179
0.0091


a
LPO^WT
LPO^FGF21
cTEC
mTEC
30.8%
28.4%
30.2%
28.9%
Ki67
FSC-A
b
cTECs
mTECs
ns
ns
% Ki67+
50
40
30
20
10
0
LPO^WT
LPO^FGF21
c
LPO^WT
LPO^FGF21
cTEC
mTEC
20.6%
17.6%
11.6%
13.4%
LIVE/DEAD Blue
Annexin V
d
cTECs
mTECs
ns
ns
% Annexin V+
40
30
20
10
0
20
15
10
5
0
LPO^WT
LPO^FGF21


a
cTEC
2.5 weeks
3 months
12 months
MFI p4EBP1
0.0224
LPOWT LPOFGF21
b
MFI pAktS473
0.0085
0.0024
c
mTEC
0.0156
0.3778
0.1391
d
0.6109
0.2543
0.3614
e
Lymphocytes
0.5741
0.9931
0.7764
f
0.2779
0.6487
0.8184


105
100
95
90
85
80
Body Weight
(% baseline)
0
1
2
3
4
5
6
7
8
9
10
11
Days post IAV PR8 infection
LPO^WT
LPO^FGF21
**
**
*


a
2 month
12 month
CD8⁺ SP
Vβ2⁺
Vβ7⁺
Vβ8⁺
Vβ11⁺
3.15%
9.24%
1.74%
4.89%
2.27%
9.79%
4.69%
7.12%
CD8
CD4
Vβ2
Vβ7
Vβ8
Vβ11
b
c
d
e
% Vβ2⁺ (CD8⁺)
% Vβ7⁺ (CD8⁺)
% Vβ8⁺ (CD8⁺)
% Vβ11⁺ (CD8⁺)
2 mo
12 mo
LPOWT
LPOFGF21